



저작자표시-비영리-변경금지 2.0 대한민국

이용자는 아래의 조건을 따르는 경우에 한하여 자유롭게

- 이 저작물을 복제, 배포, 전송, 전시, 공연 및 방송할 수 있습니다.

다음과 같은 조건을 따라야 합니다:



저작자표시. 귀하는 원저작자를 표시하여야 합니다.



비영리. 귀하는 이 저작물을 영리 목적으로 이용할 수 없습니다.



변경금지. 귀하는 이 저작물을 개작, 변형 또는 가공할 수 없습니다.

- 귀하는, 이 저작물의 재이용이나 배포의 경우, 이 저작물에 적용된 이용허락조건을 명확하게 나타내어야 합니다.
- 저작권자로부터 별도의 허가를 받으면 이러한 조건들은 적용되지 않습니다.

저작권법에 따른 이용자의 권리는 위의 내용에 의하여 영향을 받지 않습니다.

이것은 [이용허락규약\(Legal Code\)](#)을 이해하기 쉽게 요약한 것입니다.

[Disclaimer](#)

Distinctive skin microbe-dependent activation
of TSLP-group 2 innate lymphoid cells
priming axis in early neonatal stage is co-
opted in allergic skin inflammation

Jimin Cha

Department of Medical Science

The Graduate School, Yonsei University

Distinctive skin microbe-dependent activation
of TSLP-group 2 innate lymphoid cells
priming axis in early neonatal stage is co-
opted in allergic skin inflammation

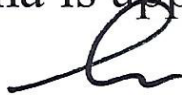
Directed by Professor Ji-Hwan Ryu

The Doctoral Dissertation
submitted to the Department of Medical Science,
the Graduate School of Yonsei University
in partial fulfillment of the requirements for the degree of
Doctor of Philosophy in Medical Science

Jimin Cha

December 2023

This certifies that the Doctoral Dissertation
of Jimin Cha is approved.



Thesis Supervisor: Ji-Hwan Ryu



Thesis Committee Member#1: Tae-Gyun Kim



Thesis Committee Member#2: Hye Young Kim



Thesis Committee Member#3: Do Young Kim



Thesis Committee Member#4: Sang Sun Yoon

The Graduate School
Yonsei University

December 2023

ACKNOWLEDGEMENTS

Infinite thanks and glory to my Lord God for allowing me to study. I would like to express deep gratitude for my supervisor Professor Ji-hwan Ryu for his unstinting support, honorable instruct and advice throughout my PhD research studies but also my future plan. In addition, I would like to send sincerely appreciate about Professor Ji-hwan Ryu for giving me the opportunity to conduct the research I want to do. And I am deeply grateful to the members of my PhD committee, Professor Tae-Gyun Kim, Hye Young Kim, Do Young Kim and Sang Sun Yoon for their respectable advice and suggestion. And I also gratefully acknowledge encouragement and guidance about research of Professor Tae-Gyun Kim. I appreciate to Professor Mina Rho for her splendid bioinformatics analysis.

I would like to thank all of generous and considerate colleagues of my lab including Professor Chang-Hoon Kim and Dr. Youn Wook Chung.

I am deeply indebted to my friends Inhwa, Wool, Shinyoung, hyewon and Eunbin for their endless and unstinted encouragement.

I am sincerely grateful to the pastor and church family who always prayed for me.

Most importantly, I would like to thank and send love all my family particularly my parents, husband, sister, grandparents and parents in law for their unconditional love, support and encouragement.

<TABLE OF CONTENTS>

ABSTRACT	vi
I. INTRODUCTION	1
II. MATERIALS AND METHODS	4
1. A. Mice	4
B. Production of <i>Tslp</i> -null transgenic mouse	4
2. Bacterial strain, culture and mouse association	5
3. Construction of ArAT mutant strains in <i>Staphylococcus aureus RN4220</i>	5
4. Mouse atopic dermatitis (AD) model and index	6
5. Antibiotics treatment	7
6. Antibody treatment in vivo	7
7. Measurement of skin microbe	8
8. Topical IAld treatment in mice	8
9. Skin cell preparation	9
A. ILCs and T cells	9
B. Keratinocytes	9
10. Flow Cytometry Analysis	10
A. ILCs	10
B. T cells	11
C. Keratinocytes	11
11. ILC adoptive transfer	11
12. Two-photon microscopy	12
13. Single cell RNA sequencing and analysis	12
14. RNA seq and analysis	13
15. DNA extraction from skin microbiota	15
16. Library construction and Sequencing	15
17. Analysis of 16S rRNA gene sequencing	16

18. Whole genome sequencing of <i>S. lentus</i>	16
A. Sequel library construction	17
B. Truseq DNA Nano (350) Library construction	17
19. Analysis of bacterial whole genome sequencing	17
20. Mono-association with bacteria in mice	18
21. Preparation of <i>S. lentus</i> for in vitro treatment	18
22. Tape stripping of mouse skin	19
23. Quantification of tryptophan metabolites	19
24. HaCaT cell culture	20
25. RNA isolation and quantitative polymer chain reaction	20
26. Quantification and statistical analysis	21
III. RESULTS	22
1. AD-like skin inflammation is attenuated by constitutive deficiency of commensal microbiota	22
2. Microbiota colonization during specific neonatal window induces cutaneous ILC2 priming	28
3. Microbiota-induced TSLP production in keratinocytes is responsible for postnatal ILC2 priming	34
4. The early postnatal skin commensal microbe <i>Staphylococcus lentus</i> sufficiently induces TSLP production and ILC2 priming	41
5. Tryptophan metabolite IAld-producing Staphylococcal species induce postnatal TSLP production and ILC2 priming	46
6. Early postnatal <i>S. lentus</i> -TSLP-ILC2 priming axis is co-opted in AD-like inflammation in adults	51
IV. DISCUSSION	63
V. CONCLUSION	66
REFERENCES	67
ABSTRACT(IN KOREAN)	77

LIST OF FIGURES

Figure 1. Commensal microbiota is responsible for pathophysiology in MC903-induced AD-like allergic skin inflammation	24
Figure 2. AD-like skin inflammation is attenuated by constitutive deficiency of commensal microbiota	26
Figure 3. Microbiota colonization during specific neonatal window induces cutaneous ILC2 priming	30
Figure 4. Cutaneous ILC2 priming during specific neonatal window is responsible for pathophysiology in MC903-induced AD-like allergic skin inflammation	32
Figure 5. Microbiota-induced TSLP production in keratinocytes is responsible for postnatal ILC2 priming	37
Figure 6. TSLP in KCs is responsible for postnatal ILC2 maturation and priming in a skin microbiota-dependent manner, whereas IL-18 and CCL20/CCR6 induce ILC2 and ILC3 priming in a skin microbiota-independent manner	39
Figure 7. Early postnatal skin commensal microbe <i>Staphylococcus lentus</i> sufficiently induces TSLP production and ILC2 priming	43
Figure 8. Clearly distinct skin commensal microbe <i>Staphylococcus lentus</i> induces TSLP production and ILC2 priming during specific neonatal window	44
Figure 9. Tryptophan metabolite IAld-producing Staphylococcal	

species induce postnatal TSLP production and ILC2 priming	48
Figure 10. Amino acid metabolism-related genes in Staphylococcal species and mutant strain for <i>S. aureus</i> deficient in ArAT ...	50
Figure 11. Early postnatal <i>S. lentus</i> -TSLP-ILC2 priming axis is co- opted in AD-like inflammation in adults.....	54
Figure 12. Bacterial unicity for IAld-producing potential leading to predisposition to AD-like inflammation	56
Figure 13. Neonatal skin microbe-TSLP-ILC2 priming axis contributes to AD-like inflammation in adulthood	58
Figure 14. Different extent of postnatal ILC2 priming between SPF and GF skin leads to different severity of AD-like inflamm- ation.....	59
Figure 15. Skin microbe-dependent TSLP-ILC2 Priming Axis in early life is co-opted in allergic inflammation	61

LIST OF TABLES

Table 1. Primers used in this study	62
---	----

ABSTRACT

Distinctive skin microbe-dependent activation of TSLP-group 2 innate lymphoid cells priming axis in early neonatal stage is co-opted in allergic skin inflammation

Jimin Cha

*Department of Medical Science
The Graduate School, Yonsei University*

(Directed by Professor Ji-Hwan Ryu)

Although early life colonization of commensal microbes contributes to long-lasting immune imprinting in host tissues, little is known regarding the pathophysiological consequences of postnatal microbial tuning of cutaneous immunity. Here, we show that postnatal exposure to specific skin commensal *Staphylococcus lentus* (*S. lentus*) promotes the extent of atopic dermatitis (AD)-like inflammation in adults through priming of group 2 innate lymphoid cells (ILC2s). Early postnatal skin is dynamically populated by discrete subset of primed ILC2s driven by microbiota-dependent induction of thymic stromal lymphopoietin (TSLP) in keratinocytes. Specifically, indole-3-aldehyde-producing tryptophan metabolic pathway, shared across *Staphylococcus* species, is involved in TSLP-mediated ILC2 priming. Furthermore, we demonstrate a critical contribution of the early postnatal *S. lentus*-TSLP-ILC2 priming axis in facilitating AD-like inflammation that is not replicated by later microbial exposure. Thus, our findings highlight the fundamental role of time-dependent neonatal microbial-skin crosstalk in shaping the threshold of innate type 2 immunity co-opted in adulthood.

Key words : allergic skin inflammation, atopic dermatitis, early postnatal life, group

2 innate lymphoid cells, priming, skin microbiota, staphylococcus, tryptophan metabolites

Distinctive skin microbe-dependent activation of TSLP-group 2 innate lymphoid cells priming axis in early neonatal stage is co-opted in allergic skin inflammation

Jimin Cha

*Department of Medical Science
The Graduate School, Yonsei University*

(Directed by Professor Ji-Hwan Ryu)

I. INTRODUCTION

The barrier surfaces of living organisms harbor distinct communities of symbiotic microbes with temporal and topographical dynamics.^{1,2} At the forefront of host defense, skin is the outermost epithelial organ that provides physical and immunological protection.^{3,4} A series of mouse studies have shown that skin is associated with a diverse community of commensal microbes that play essential roles in maintaining functional homeostasis.^{5,6} Skin commensal microbes facilitate the expression of skin barrier-related genes and recovery of the skin barrier.^{7,8} In addition, skin commensals promote wound healing and wound-induced hair follicle neogenesis through the inflammatory and metabolic regulation of keratinocytes (KCs).^{9,10} Besides, skin microbiome also plays a distinct role in fine-tuning of the cutaneous immune responses.¹¹ Recent studies show that germ-free (GF) mice revealed a reduced inflammatory response to ultraviolet radiation and IL-1 β -dependent skin wound healing, suggesting that commensal microbiota augments skin inflammation.⁹ ¹² Furthermore, colonization with *Staphylococcus epidermidis* (*S. epidermidis*), one of the commensal *Staphylococci* present on human and mouse skin, induces commensal-specific IL-17A⁺CD8⁺ T cells, which in turn provides the protective immunity against pathogens and accelerate skin wound repair.¹³⁻¹⁶ Therefore, a deeper understanding of the skin

microbiota-host immune interaction is crucial for translating skin immune response and physiology in health and disease.

Several mouse studies have demonstrated that exposure to the commensal microbiome early in life contributes to the enduring effects of skin immune imprinting, leading to consequent functional changes in long-term immunity and physiology.^{17, 18} Colonization with *S. epidermidis* in neonatal mice induces the expansion of *S. epidermidis*-specific regulatory T cells (Tregs), which provide immune tolerance upon subsequent challenge of same bacteria in adults.¹⁹⁻²¹ In addition, the development of cutaneous mucosal-associated invariant T cells is determined by exposure to microbes that synthesize riboflavin-derived antigens early in the postnatal period, which results in an accelerating wound repair in adult life.²² However, recent studies have also demonstrated that early life colonization with certain microbes is associated with the development of inflammatory skin diseases such as atopic dermatitis (AD). Postnatal developing human skin displays dynamic changes in composition of commensal microbial community, dominated by colonization of *Staphylococci*.²³ Among skin commensal *Staphylococci*, several human cohort studies have shown that early colonization of *Staphylococcus aureus* (*S. aureus*) precedes the diagnosis of AD and promotes predisposition to AD.^{24, 25} However, the mechanistic understanding of how microbial coordination of cutaneous immunity early in life contributes to the magnitude of the skin immune response in adulthood is largely unknown. Microbiota-derived metabolic derivatives, such as tryptophan (Trp) metabolites, have critical roles in immune cell maturation, imprinting, and fine-tuning of local inflammatory milieu.²⁶⁻³⁰ Microbial Trp metabolites, including indole and indole-3-aldehyde (IAld), lead to immune balance of gut mucosa in mouse through supporting the integrity of gut epithelial cells and inducing interleukin (IL)-22 production from group 3 innate lymphoid cells (ILC3s).³¹⁻³³ The metabolic function of the skin microbiome is distinct from that of the gut microbiome due to limited metabolic substrates under the harsh skin environment.^{5, 6} In the human AD lesional skin, the Trp metabolic pathway is attenuated in skin microbiota,³⁴ and topical treatment of IAld attenuates murine model of AD-like inflammation through suppression

of thymic stromal lymphopoietin (TSLP) expression.³⁵ However, it is largely unclear whether skin commensal-derived metabolites are actively involved in early postnatal immune imprinting under homeostatic conditions.

Here, we show that cutaneous group 2 ILCs (ILC2s) undergo dynamic postnatal priming during the first few weeks of life depending on the skin commensal microbiome. Based on temporal analyses of transcriptome and microbial communities, we demonstrate that early colonization by *Staphylococcus lentus* (*S. lentus*) is sufficient to drive ILC2 priming through inducing TSLP in postnatal KCs. Skin commensal *Staphylococci* share a unique metabolic pathway for Trp metabolites, and IAld-synthesizing *Staphylococcus* promotes TSLP-dependent ILC2 priming. Consequently, skin microbe-dependent TSLP-ILC2 priming axis is co-opted in AD-like inflammation in adult mice. Therefore, this work highlights the fundamental role of time-dependent microbial-skin crosstalk in shaping the threshold of innate type 2 immunity, which provides a potential neonatal window for regulating the magnitude of allergic inflammation.

II. MATERIALS AND METHODS

1.

A. Mice

Wild-type (C57BL/6), *Tslp*-null transgenic (C57BL/6), *Rag1*-null (C57BL/6), *Ccr6*-null (C57BL/6), and CD45.1 (C57BL/6) mice were housed under SPF conditions. GF mice (C57BL/6) were housed and maintained in the gnotobiotic animal facility in Yonsei University College of Medicine. Sex- and age-matched mice between 8 and 12 weeks of age were used for each experiment. In all neonate experiments, mice between 0 and 28 days of age were used. All experiments were performed in accordance with the Association for Assessment and Accreditation of Laboratory Animal Care International (AAALAC International) guidelines and approved by the Institutional Review Board of the Yonsei University College of Medicine (approval number: 2018-0308 or 2021-0049).

B. Production of *Tslp*-null transgenic mouse

Mouse zygotes were collected from super-ovulated C57BL/6N females as described previously³⁶. Briefly, female C57BL/6N mice at 5-6 weeks of age were injected with 5 IU of pregnant mare serum gonadotrophin (PMSF, Sigma Aldrich, St. Louis, State of Missouri, U.S.), followed by 5 IU of human chorionic gonadotropins (Hcg, Sigma Aldrich, St. Louis, State of Missouri, U.S.) 48 h apart, and mated with C57BL/6N male mice. Successful mating was determined the following morning by detection of a vaginal plug. Mouse zygotes were transferred to M2 medium (Sigma Aldrich) containing 0.1% (w/v) hyaluronidase to remove cumulus cells and cultured in M16 medium (Sigma Aldrich) at 37°C, 5% CO₂ in air before microinjection.

Single-guide RNAs (sgRNAs) and recombinant Cas9 protein were purchased from ToolGen. The sgRNA-1 and -2 sequences targeting *Tslp* gene were 5'-AGTTGAAGCAAA CTGATGGTAGG-3' and 5'-TGCAAGTACTAGTACGGATGGGG-3', respectively. Cas9 protein and sgRNAs were mixed using microinjection buffer (0.1 mM EDTA/10 mM Tris-Cl, pH 7.4) to the final concentration of 40 ng/μl each and incubated for 15 min at 37 °C

immediately before microinjection³⁷. Microinjection was performed 24 hr after human chorionic gonadotropin injection. To visualize the pronuclei, cumulus-free zygotes were centrifuged at 13,000 rpm for 5 min³⁶. Embryos with clearly visible pronuclei were selected, and the mixture of sgRNAs and Cas9 were injected into the male pronucleus. Microinjection was performed under an inverted microscope equipped with micromanipulator and a microinjector (Leica, Sigma Aldrich, Germany). The injected zygotes were cultured in M16 media for 48 hr and then transferred into the oviduct of a pseudopregnant foster mother (ICR). The tail-tip genomic DNAs were extracted from resultant pups and genotyped by PCR. The primers used for genotyping were 5'-CGTAGG CGTTTAGGTGTTATA-3 and 5'-TGTGATATTTGCCCTACTTT-3'.

2. Bacterial strain, culture and mouse association

Staphylococcus lentus and *Staphylococcus xylosus* were collected from SPF mouse skin. For bacterial isolation, whole skin from neonatal SPF mice was homogenized in PBS, filtered through a 40- μ m strainer, and spread on Brain Heart Infusion plates (BHI, BD Biosciences, Franklin Lakes, New Jersey, U.S.). After overnight incubation, colonies were identified using capillary electrophoresis sequencing by MacroGen (Seoul, Korea). *Staphylococcus lentus*, *Staphylococcus xylosus*, and *Staphylococcus epidermidis* strains were grown for 18 h in tryptic soy broth (TSB [BD Biosciences, Franklin Lakes, New Jersey, U.S.]) at 37 °C, to a density of approximately 10⁹ colony-forming units (CFUs)/mL. *Staphylococcus aureus* RN4220 was grown for 18 h in Brain Heart Infusion broth (BHI [BD Biosciences]) and *Staphylococcus aureus* Δ ArAT were grown for 18 h in BHI broth at 37 °C with 10 μ g/ml erythromycin. *Escherichia coli* was grown for 18 h in LB broth (Tryptone 10 g/mL, Yeast 5 g/mL, NaCl 10 g/mL) at 37 °C.

3. Construction of ArAT mutant strains in *Staphylococcus aureus* RN4220

For generation of ArAT gene mutation by erythromycin insertion, 883 bp fragment upstream and 766 bp fragment downstream of ArAT were amplified from *S. aureus* RN4220

genome using primers pairs ArAT_900_Fw/ ArAT(N177)_Erm_Rv and Erm_ArAT(N177)_Fw / ArAT_780_Rv, which are inserted into pENTR/D-TOPO vector (Life Technologies, Carlsbad, California, U.S.), respectively. A erythromycin B cassette was amplified from plasmid pCD256ΔEC_Ptuf34_mCherry using primer pair ArAT(N177)_Erm_Fw /Erm_ArAT(N177)_Rv.³⁸ Purified PCR products were then fused by splice overlap extension PCR using primers ArAT_900_Fw/ ArAT_780_Rv. The PCR product was subcloned into pENTR/D-TOPO plasmid. ArAT::Erm^R_pENTR was recombined with pKOR1(Addgene, Watertown, Massachusetts, U.S.)- an *E. coli*/ *S. aureus* shuttle vector- by LR Clonase (Thermofisher Scientific, Waltham, MA, U.S.), making pKOR1_ArAT::Erm. The resulting plasmid was subsequently electroporated into *S. aureus RN4220* and stably maintained at 30 °C on BHI agar plate with 10 ug/ml chloramphenicol and 5 ug/ml erythromycin (BHI_{Cm10/Erm5}), Generating *S. aureus RN4220* (pKOR1_ArA-T::Erm). *ArAT* allele replacement was carried out by a two-step procedure as described before with minor modifications.³⁹ In the first step, plasmid was integrated into the chromosome by staphylococcal growth at the non-permissive condition. 5 ul of *S. aureus RN4220* (pKOR1 pKOR1_ArAT::Erm) culture grown at 30 °C in BHI_{Cm10/Erm5} broth was inoculated into 5ml of fresh BHI_{Cm10/Erm5} broth and incubated overnight in shaking incubator at 43 °C. The following day, the culture was plated on BHI_{Cm10/Erm5} agar media and incubated at 43 °C overnight. One colony from the plate was cultured in BHI_{Cm10/Erm5} broth at 30 °C overnight to facilitate plasmid excision. Culture was spread on BHI_{Erm5} agar containing 2 ug/ml anhydrotetracycline(ATc) and incubated at 30 °C for 2 days for pKOR1 excision and loss. To identify *S. aureus RN4220 ArAT::Erm mutant*, 5 colonies were tested by PCR amplification using specific primer set ArAT mut 100 Fw /ArAT mut 486 Rv (mutant: 3363 bp, wildtype: 2240 bp) and subsequently confirmed by sequencing the PCR product DNA.

4. Mouse atopic dermatitis (AD) model and index

To establish the atopic dermatitis model, mice ears were treated once daily with 2 nmol of MC903 (Calcipotriol, Tocris Bioscience, Bristol, UK) in 20 μL of ethanol.⁴⁰ Ear

thickness was daily measured using a dial thickness gauge (PEACOCK, Ozaki MFG Co. Ltd., Tokyo, Japan). After 5 or 7 days of MC903 treatment, ear skin was harvested for measuring ear thickness, accumulated leukocyte number, and local gene expression. The ear skins were fixed in 4% paraformaldehyde (PFA) (Biosesang, Seongnam, Korea) and embedded in paraffin before sectioning (4 μ m thick sections) and staining with Hematoxylin & Eosin (H&E). Epidermal thickness was analyzed using ImageJ software (NIH, Bethesda, MD, U.S.). H&E Images were acquired using light microscope (Zeiss) and analyzed by Image J. Leukocyte number was counted in H&E images in same fields.

5. Antibiotic treatment

Intestinal bacteria ablation in adult SPF mice was achieved via treatment with an antibiotics cocktail comprising 0.1 g/L of vancomycin (Sigma Aldrich), 0.1 g/L of ampicillin (Sigma Aldrich) and 0.1 g/L of metronidazole (Sigma Aldrich). Antibiotics were added into drinking water for 14 days. Skin bacteria ablation in adult mice was achieved via topical treatment with antibiotic ointment (Neosporin: triple antibiotic ointment, 1 g containing: bacitracin 400 units, neomycin 3.5 mg and polymyxin B 5000 units) (Johnson & Johnson consumer inc., New Brunswick, New Jersey, U.S.) of mouse ear skin. 10 min after MC903 treatment, Neosporin treatment was applied to dry skin. This treatment was repeated for 7 consecutive days. For neonatal skin microbiota ablation, Neosporin was applied to the entire skin once daily to neonatal mice at P1, the skin of the mice was assessed at P14.

6. Antibody treatment in vivo

Adult SPF mice were intraperitoneally administered with 300 μ g of anti-CD4 (Bio X cell, Lebanon, NH, U.S.) or Rat IgG2b (Bio X cell) for consecutive 2 days before treatment with MC903. SPF *Rag-null* mice were intraperitoneally administered 8 μ g/g anti-CD25 (Bio X cell) or Rat IgG1 (Bio X cell) for 4 days at P4, P5, P8, and P11. Both groups were treated with MC903 to establish the AD-like skin inflammation model in adults (P56). SPF

neonatal mice were intraperitoneally administered 8 $\mu\text{g/g}$ anti-IL-7R α (Bio X cell), anti-IL-7 (Bio X cell), anti-TSLP (R&D systems, Minneapolis, MN, U.S.), and anti-IL-18Ra (R&D systems) or corresponding isotype antibodies, including Rat IgG2a (Bio X cell), Mouse IgG2b (Bio X cell), and Rat IgG2a (R&D systems), for 4 days at P4, P5, P8, and P11, then skin was harvested at P14 for further analysis.

7. Measurement of skin microbe

To measure the abundance of skin microbiota, skin, which was not shaved and not applied any hair removal cream, was obtained from the ears of mice, and homogenized in 2 mL of PBS. The ear skin suspension was then filtered through 40- μm strainers and spread on tryptic soy agar plates with 5% sheep blood (Kisan bio, Seoul, Korea). Colonies were counted after overnight incubation in a 37 °C bacterial oven. In addition, mouse whole body skin, which was not shaved hair and not applied any hair removal cream, were rubbed with sterile swabs saturated with lysis buffer (20 mM Tris, pH 8.0, 2 mM EDTA, 1.2% Triton X-100 and lysozyme [20 mg/mL]).⁴¹ Bacterial DNA was extracted from the swabs using PureLink™ RNA Mini Kit (Invitrogen™, Waltham, Massachusetts, U.S.) following the manufacturer's instructions. For quantification of total skin bacteria and *S. lentus*, quantitative PCR was conducted on QuantStudio 3 Real-Time PCR (Life technologies) using KAPA SYBR® FAST ABI Prism® (Kapa biosystems, Station Cl, UK). Quantification of total skin bacteria and *S. lentus* was determined by the comparative $2^{-\Delta\text{CT}}$ method. Total skin bacteria were determined using PCR primer 16S_27F 5'-AGAGTTTGATCCTGGCTCAG-3' and 16S_534R 5'-ATTACCGCGGCTGCTGG-3'.

8. Topical IAld treatment in mice

Neonate mice were topically treated with 0.5 mM IAld (Sigma) or ethanol (vehicle) over the entire skin surface. Treatment was repeated every other day for a total of four times at P5, P7, P9, and P11, then skin was harvested at P14 or P56. In some experiments, GF mice

were exposed to IAId a total of four times at P28, P30, P32, and P34. For the consecutive association of *S. lentus* following topical IAId treatment, neonate mice were treated with 0.5 mM IAId or ethanol (vehicle) over the entire skin surface for a total of four times at P5, P7, P9, and P11, and 3 mL of *S. lentus* culture suspension was applied over the entire skin surface using a sterile swab for a total of four times at P28, P30, P32, and 34. Subsequently, P56 mice were treated with MC903 to assess AD-like skin inflammation.

9. Skin cell preparation

A. ILCs and T cells

Skin cell suspensions were prepared from mouse whole body skin. Hair was shaved with electric clippers and removed with hair removal cream (Church & Dwight Co., Inc., Ewing, New Jersey, U.S.). Large pieces of subcutaneous fat were mechanically removed with forceps. To quantify total ILCs, IL-5⁺ ILC2s, and IL-17A⁺ ILC3s, skin tissues were minced into small pieces and digested with 1.7 mg/mL Collagenase A (Roche, Basel, Switzerland) in RPMI-1640 (Lonza, Basel, Switzerland) for 120 min at 37 °C with shaking every 20 min. Subsequently, digested skin samples were passed through 70- μ m strainers to obtain single-cell suspensions. To analyze CD25⁺ ILCs, T-bet⁺ ILC1s, GATA3⁺ ILC2s, ROR γ t⁺ ILC3s, and T cells, skin tissues were minced and digested with 0.25 mg/mL Liberase T-flex (Roche) in RPMI-1640 (Lonza) for 120 min at 37 °C with shaking every 20 min. Subsequently, digested skin samples were dissociated through 70- μ m strainers to obtain single-cell suspensions. To determine cytokine production potential, the single-cell suspensions were stimulated *ex vivo* for 3 h at 37 °C and 5% CO₂ with 1:500 dilution of PMA/ionomycin/Brefeldin A cocktail (Biolegend, San Diego, California, U.S.) in 12-well plates and 2 mL of RPMI (RPMI-1640 with 10% FBS (Gibco, Waltham, Massachusetts, U.S.), 1% antibiotics [100 U/mL penicillin/streptomycin (Gibco)] and 0.05 mM β -mercaptoethanol [Gibco]). The cells were then analyzed via flow cytometry.

B. Keratinocytes

Skin cell suspensions were prepared from mouse whole body skin. Hair was shaved with electric clippers and removed with hair removal cream. Subcutaneous tissues were mechanically removed with forceps. Skin tissues were floated in 2 mg/mL dispase II (Roche) and incubated at 37 °C for 40 min–1 h. The epidermis was then scraped off with forceps, minced and incubated with trypsin-EDTA (0.25%; Gibco) at 37 °C for 10 min. The epidermal cell suspension was mechanically dissociated with a 3-mL syringe (KOVAX, Seoul, Korea) and 19-gauge needle (KOVAX), then filtered through a 70- μ m strainer. Single cells were analyzed via flow cytometry for cell sorting.

10. Flow cytometry analysis

A. ILCs

ILCs were stained with anti-mouse CD45 (1:500, 103134, BioLegend), Thy1.2 (1:500, 140309, BioLegend), CD25 (1:100, BioLegend), CD218 (1:100, [eBioscience, Waltham, MA, U.S.]) and lineage marker (1:100, BioLegend) antibodies for 30 min at 4 °C. For intracellular cytokine staining, cells were fixed and permeabilized with BD Cytofix/Cytoperm and washed with BD Perm Wash buffer (BD Biosciences). They were then stained with anti-mouse IL-5 (1:100, 61-7133-82, eBioscience) and IL-17A antibodies (1:100, 506908, BioLegend) for 30 min at 4 °C. For transcription factor staining, cells were fixed and permeabilized with the Foxp3/Transcription Factor Staining Buffer Set (eBioscience) and stained with anti-mouse GATA3 (1:100, 61-9966-42, eBioscience), ROR γ t (1:100, 17-6981-82, eBioscience), and T-bet (1:100, 644817, BioLegend) antibodies for 30 min at 4 °C. Single cells were used for analysis and CD45⁺ cells were gated as hematopoietic cells. Lineage markers (BioLegend) were used to distinguish ILCs from other immune cells and included CD2 (100116), CD3 ϵ (100328), CD5 (100624), CD19 (115534), CD11c (117328), CD11b (101228), Fc ϵ RIa (134320), TCR $\gamma\delta$ (118118), TCR $\alpha\beta$ (109228), NK1.1 (108728) and B220 (103236). IL-5⁺ ILC2s were gated as CD45⁺Lin⁻Thy1.2⁺IL-5⁺; IL-17A⁺ ILC3s were gated as CD45⁺Lin⁻Thy1.2⁺IL-17A⁺; CD25⁺ ILCs were gated as CD45⁺Lin⁻Thy1.2⁺CD25⁺; IL-18R α /CD218⁺ primed ILC2s

were gated as $CD45^+Lin^-Thy1.2^+IL-5^+CD218^+$; T-bet⁺ ILC1s were gated as $CD45^+Lin^-Thy1.2^+CD3\epsilon^-T-bet^+$; GATA3⁺ ILC2s were gated as $CD45^+Lin^-Thy1.2^+CD3\epsilon^-GATA3^+$; ROR γ t⁺ ILC3s were gated as $CD45^+Lin^-Thy1.2^+CD3\epsilon^-ROR\gamma t^+$. ILCs were sorted as $CD45^+Lin^-Thy1.2^+$ for single-cell RNA sequencing and adoptive transfer by AriaIII (BD Biosciences). The data was gained by LSR Fortessa (BD Biosciences) and analyzed using FlowJo software (FlowJo, LLC).

B. T cells

Th2 and Treg cells were stained with CD45, Thy1.2, lineage markers, and CD3 ϵ (1:100, 100355, BioLegend) antibodies for 30 min at 4 °C. For transcription factor staining, cells were fixed and permeabilized with the Foxp3/Transcription Factor Staining Buffer Set and stained with anti-mouse GATA3 and Foxp3 (1:100, 25-5773-82, eBioscience) antibodies for 30 min at 4 °C. For intracellular cytokine staining, cells were fixed and permeabilized with BD Cytofix/Cytoperm and washed with BD Perm Wash buffer. Then cells were stained with anti-mouse IL-5, IL-4(1:100, 12-7041-41, eBioscience) and IL-13 (1:100, 12-7133-41, eBioscience) for 30 min at 4 °C. Single cells were used for analysis and $CD45^+$ cells were gated as hematopoietic cells. Lineage markers were used to distinguish T cell from other immune cells and comprised CD19, CD11c, CD11b, Fc ϵ RIa, TCR $\gamma\delta$, NK1.1, and B220. Th2 cells were gated as $CD45^+Lin^-Thy1.2^+CD3\epsilon^+GATA3^+$ or $CD45^+Lin^-Thy1.2^+CD3\epsilon^+IL-4^+IL-5^+IL-13^+$ while Tregs were gated as $CD45^+Lin^-Thy1.2^+CD3\epsilon^+Foxp3^+$. The data was gained by LSR Fortessa and analyzed using FlowJo software.

C. Keratinocytes

Epidermal single cells were stained with anti-mouse CD45.2 antibody (BioLegend) and PI (propidium iodide [BioVision, Waltham, MA, U.S.]) for 30 min at 4 °C. KCs were sorted as $PI^-CD45.2^-$ by AriaIII (BD Biosciences).

11. ILC adoptive transfer

Cells were isolated from neonatal skin of SPF WT, GF, SPF *Tslp*^{-/-} mice. Toal skin ILCs ($CD45^+Lin^-Thy1.2^+$) were sorted by AriaIII (BD Biosciences) after enrichment of

lymphocytes using mouse CD45 micro beads (Miltenyi Biotec, Bergisch Gladbach, Germany). Adult GF mice were intradermally injected with 5,000–7,000 (9,000–10,000 for normalized GF ILCs) sorted ILCs in the bilateral ear skin. One day after ILC transfer, ear skin was harvested for flow cytometric analysis of CD45.2⁺ host ILC2s and Th2 cells. In addition, ILC-transplanted mice were treated with MC903 to induce AD-like skin inflammation and further analysis.

12. Two-photon microscopy

Skin single cells were isolated from neonatal skin of SPF mice. Cells were labeled with 10 μ M of CellTracker Red CMTPX Dye for 30 min at room temperature. Subsequently, ILCs (CD45⁺Lin⁻Thy1.2⁺) were sorted by AriaIII (BD Biosciences) after enrichment of lymphocytes using mouse CD45 micro beads (Miltenyi Biotec). Adult GF mice were intradermally injected with 9,000–15,000 sorted ILCs in the ear skin. 24 h after ILC transfer, the ear was spread on the silicone bed and covered with a slide glass in the imaging chamber. Two-photon microscopy was performed using FVMPE-RS laser scanning microscope (Olympus) equipped with a X25 NA 1.05 water immersion objective lens. For two-photon excitation, the InSight DeepSee pulsed IR laser systems were adjusted to 880 nm to visualize second harmonic generation (SHG), green, and red channels. Images were acquired at a resolution of 512 x 512 pixels, capturing z-stack and time series data using a galvanometer scanner. The video was edited using Volocity software v6.3.1 (PerkinElmer, Waltham, Massachusetts, U.S.) and was converted using the Movavi video editor program (Movavi).

13. Single cell RNA sequencing and analysis

ILCs were sorted from mouse whole body skin as CD45⁺Lin⁻Thy1.2⁺ (Lin: CD2, CD3e, CD5, CD19, CD11c, CD11b, Fc ϵ RIa, TCRgd, TCRab, NK1.1, CD2, and B220). Samples were pooled, encapsulated into droplets using the Chromium Single Cell Controller (10X

Genomics, Pleasanton, California, U.S.), and libraries were prepared using the Chromium Next GEM Single Cell 3p RNA library v3.1 (10X Genomics) per the manufacturer's protocol. Barcoded libraries were sequenced with the Hi-Seq XTen platform and raw data were processed using the standard Cell Ranger pipeline (ver.3.1.0, 10X Genomics). Analysis of the raw gene expression matrices was performed using Seurat package (ver.4.1.0) according to the standard workflow. Briefly, we included cells that met the filtration criteria, (1) number of genes between > 200 and < 6000 , and (2) $< 20\%$ of mitochondrial gene expression. We then performed normalization, integration, and scaling. Cells were clustered by PCA followed by Seurat FindCluster function with a resolution of 0.4. Cellular annotation was performed by unbiased approaches based on the profiling of differentially expressed genes (DEGs) for each cluster using the Seurat FindMarkers function, which presented several cell type-specific genes to define cell identity. After removing doublets, ILC cluster analysis was performed according to the standard pipeline applied to the whole cells. The final cell numbers were 1471 for P1 ILCs and 3775 for P14 ILCs, respectively. Trajectory analysis was performed using the Monocle 2 package according to the standard workflow. KEGG pathway analysis of upregulated genes in primed ILC2 compared to other ILC subsets (\log_2 fold change > 0.3 and q -value < 0.05) was performed using a web based g:Profiler functional enrichment tool (<https://biit.cs.ut.ee/gprofiler/gost>). Raw data for scRNA-seq were deposited in the Gene Expression Omnibus (GEO) database under accession number GSE214848.

14. RNA seq and analysis

Total skins were isolated from the ear skin of SPF and GF mice treated with ethanol or MC903 for 5 days. RNA was prepared using the RNeasy® Fibrous Tissue Mini Kit (Qiagen, Hilden, Germany) following the manufacturer's instructions. RNA libraries were generated using TruSeq mRNA Sample Prep Kit v2 (Illumina, San Diego, California, U.S.), and the samples were sequenced on a HiSeq 4000 platform (Illumina). Keratinocytes (CD45.2⁻ PI⁻) were isolated from the whole skin of C57BL/6J mice on P1, 7, and 14. RNA was isolated

using the RNeasy® Mini Kit (Qiagen) following the manufacturer's instructions. RNA libraries were generated using the TruSeq Stranded mRNA LT Sample Prep Kit (Illumina), and samples were sequenced on a NovaSeq 6000 System User Guide Document #1000000019358 v02 (Illumina) with the NovaSeq 6000 S4 Reagent Kit (Illumina). The raw reads from the sequencer were preprocessed to remove low-quality, and adapter sequences before analysis and the processed reads were aligned to the *Mus musculus (mm10)* using HISAT v2.1.0.⁴² HISAT utilizes two types of indexes for alignment (a global, whole-genome index and tens of thousands of small local indexes). These two types of indexes are constructed using the same BWT (Burrows–Wheeler transform) graph FM index (GFM) as Bowtie2. Due to its use of these efficient data structures and algorithms, HISAT generates spliced alignments several times faster than Bowtie or BWA. The reference genome sequence of *Mus musculus (mm10)* and annotation data were downloaded from the UCSC table browser (<http://genome.uscs.edu>). Transcript assembly and abundance estimation was completed with StringTie.^{43, 44} After alignment, StringTie v1.3.4d was used to assemble aligned reads into transcripts and to estimate their abundance, thereby providing the relative abundance estimates as Read Count values of transcripts and genes expressed in each sample. DEGs between two groups were analyzed by using DESeq2 package for R software. KEGG pathway analysis of upregulated genes in P14 KCs compared to P1 KCs (\log_2 fold change > 2 and q -value < 0.05) was performed using a web based g:Profiler functional enrichment tool (<https://biit.cs.ut.ee/gprofiler/gost>). Gene set enrichment analysis of differentially expressed genes (\log_2 fold change ≥ 1.5 or ≤ -1.5) between MC903-treated SPF and GF mouse skins using gene sets for Gene ontology: Biological pathway (m5.go.bp.v2023.1.Mm.symbols.gmt) was performed using GSEA software from the BROAD Institute (<https://www.gsea-msigdb.org>). Gene set variation analysis of differentially expressed genes (\log_2 fold change ≥ 1.5 or ≤ -1.5) between MC903-treated SPF and GF mouse skins using indicated gene sets was performed using GSVA package for R software. Gene sets used in GSVA analysis were retrieved from MSigDB (<https://www.gsea-msigdb.org>). Raw data for bulk mRNA-seq were deposited in

the Gene Expression Omnibus (GEO) database under accession number GSE214993 and GSE214994.

15. DNA extraction from skin microbiota

Five mice were randomly selected from separate cages (2-3 cages) at indicated time points (P7, P14, P21, P28, and P56) without longitudinal sampling from the same mouse. SPF mouse whole body skin, which was not shaved hair and not applied hair removal cream, was rubbed with sterile swabs saturated in lysis buffer (20 mM Tris, pH 8.0, 2 mM EDTA, 1.2% Triton X-100 and lysozyme [20 mg/mL])⁴¹. Each swab sample was stored at -70 °C. Negative controls were prepared with sterile swab saturated in lysis buffer without skin scrubbing. Positive controls were prepared with skin microbiome whole cell mix (ATCC, Manassas, Virginia, U.S.) according to the manufacturer's instructions. Bacterial DNA was extracted using Purelink Genomic DNA Kit (Thermo Fisher Scientific, Waltham, Massachusetts, U.S.) according to the manufacturer's instructions. The extracted DNA was quantified using Quant-IT PicoGreen (Invitrogen).

16. Library construction and Sequencing

The sequencing libraries were prepared according to the PacBio amplicon Template Preparation and Sequencing protocols to amplify the 27F and 1492R region. The input gDNA 2ng was PCR amplified with 10× LA PCR Buffer II (Mg²⁺ free), 2.5 mM of dNTP mix, 2.5 mM MgCl₂, 500 nM each of the F/R PCR primer, and 5 U of TaKaRa LA Taq (Takara, Kusatsu, Japan). The cycle condition for PCR was 5 min at 94 °C for heat activation, and 25 cycles of 30 sec at 94°C, 30 sec at 53 °C and 90 sec at 72 °C, followed by a 5-min final extension at 72 °C. The primer pairs with asymmetric barcoded adapters for the amplifications were as follows: 27-F: 5'- AGRGTTYGATYMTGGCTCAG -3', 1492-R: 5'- RGYTACCTTGTTACGACTT -3'. The PCR product was purified with SMRT bell cleanup beads. The purified product is then quantified using Quant-IT PicoGreen

(Invitrogen) and qualified using the TapeStation D5000 Screen Tape (Agilent Technologies, Waldbronn, Germany). For PacBio Sequel IIe sequencing, 500 ng of pooled amplicon DNA was used for library preparation. Total 10 uL library was prepared using PacBio SMRTbell prep kit 3.0. SMRTbell templates were annealed Sequel II Bind Kit 3.1 and Int Ctrl 3.1. The Sequel II Sequencing Kit 2.0 and SMRT cells 8M Tray was used for sequencing. SMRT cells (Pacific Biosciences, Menlo Park, California, U.S.) using 10hr movies were captured for each SMRT cell using the PacBio Sequel IIe (Pacific Biosciences) sequencing platform by Macrogen (Seoul, Korea). The subsequent steps are based on the PacBio Sample Net-Shared Protocol, which is available at <https://www.pacb.com/>.

17. Analysis of 16S rRNA gene sequencing

The bacteria composition of each sample was estimated from the full length 16S rRNA amplicon sequencing data. For quality control, the reads with minimum accuracy of > 0.99 were used. Raw data from 16S rRNA gene sequencing were deposited in the European Nucleotide Archive (ENA) database under accession number PRJEB65310. Taxonomy classification for each 16S rRNA gene sequence was performed by Kraken2⁴⁵ and bacteria composition was estimated by Bracken2.⁴⁶ The full-length 16S sequences were extracted from 32,846 bacterial complete genomes in the NCBI RefSeq database (downloaded in 2023.03.01) to build a database of Kraken2 and Bracken2. For principal coordinates analysis (PCoA), the bray-Curtis distance matrix was calculated based on the estimated bacteria composition. Calculating distance matrix and performing PCoA was performed using scikit-bio python package.

18. Whole genome sequencing of *S. lentus*

Genomic DNA of *S. lentus* was extracted by Maxwell® 16 Cell DNA Purification Kit (AS1020, Promega, Madison, Wisconsin, U.S.) following the manufacturer's instruction for both Illumina and PacBio sequencing.

A. Sequel library construction

Total 10 uL library was prepared using PacBio SMRTbell Express Template Prep Kit 2.0. SMRTbell templates were annealed using Sequel Binding and Internal Ctrl Kit 3.0. The Sequel Sequencing Kit 3.0 and SMRT cells 1M v3 Tray was used for sequencing. SMRT cells (Pacific Biosciences) using 600 min movies were captured for each SMRT cell using the PacBio Sequel (Pacific Biosciences) sequencing platform by Macrogen (Seoul, Korea). The subsequent steps are based on the PacBio Sample Net-Shared protocol, which is available at <http://pacificbiosciences.com/>. The sequencing data were converted into raw data for the analysis.

B. Truseq DNA Nano (350) Library construction

The sequencing libraries were prepared according to the manufacturer's instructions of TruSeq Nano DNA High Throughput Library Prep Kit (Illumina). Briefly, 100 ng of genomic DNA was sheared using adaptive focused acoustic technology (Covaris, Woburn, Massachusetts, U.S.) and the fragmented DNA is end-repaired to create 5'-phosphorylated, blunt-ended dsDNA molecules. Following end-repair, DNA was size selected with bead-based method. These DNA fragments go through the addition of a single 'A' base and ligation of the TruSeq DNA UD Indexing adapters. The products are then purified and enriched with PCR to create the final DNA library. The libraries were quantified using qPCR according to the qPCR Quantification Protocol Guide (KAPA Library Quantification kits for Illumina Sequencing platforms) and qualified using the Agilent Technologies 4200 TapeStationD1000 screen tape (Agilent technologies). Then sequencing was performed using HiSeqXten (Illumina) by Macrogen (Seoul, Korea). The sequencing data were converted into raw data for the analysis.

19. Analysis of bacterial whole genome sequencing

Raw DNA reads with low quality (Phred score < 20) and short length (< 90 bp) were filtered by sickle. Sequences including ambiguous nucleotides (N) were removed.

Remaining paired-end reads were assembled using MEGAHIT.⁴⁷ Only the assembled contigs with a length > 500 bp were used to predict open reading frames (ORFs) by FragGeneScan.⁴⁸ ORFs were annotated using DIAMOND⁴⁹ against KEGG⁵⁰ v98 genus prokaryotes with e-value 1e-10, similarity 40%, query coverage 40%, and subject coverage 70%. The predicted ORFs from the sequenced genome, and the genes from the NCBI complete genomes of *Staphylococcus* genus, were clustered by CD-HIT-EST⁵¹ with a 70% similarity threshold. From the clustering data, the proportion of shared genes was calculated among the species of *Staphylococcus* and 331 core genes were obtained. Multiple sequence alignment (MSA) was conducted for the core genes through Muscle.⁵² MEGA11⁵³ was used to construct a phylogenetic tree from the MSA results. Amino acid metabolic pathways were collected from KEGG module data. For the species detected in the composition analysis, the complete genomes in NCBI were downloaded and annotated using KEGG KO enzymes. Based on the number of genomes used and the enzyme annotation, the probability of the existence of each gene and each species were calculated. The pathway abundance for each species was represented using the minimum probability of essential genes in the pathway. Raw data for bacterial whole genome sequencing were deposited in the European Nucleotide Archive (ENA) database under accession number PRJEB56306.

20. Mono-association with bacteria in mice

Neonate GF mice were colonized by applying up to 1 mL of bacterial suspensions (*S. lentus*, *S. xylosum*, *S. epidermidis*, *E. coli*, *S. aureus* *WT*, and *S. aureus* Δ *ArAT*) across the entire skin surface using a sterile swab. 4 weeks of GF mice were colonized by applying up to 3 mL of bacterial suspensions across the entire skin surface using a sterile swab. Bacterial suspensions were applied a total of four times on alternate days to mouse skin at P5, P7, P9, and P11 (early association) or P28, P30, P32 and P34 (late association).

21. Preparation of *S. lentus* for *in vitro* treatment

S. lentus was cultured for 18 h in TSB media at 37 °C. *S. lentus* culture was centrifuged

at 3200 $\times g$ for 30 min. Supernatant was then filtered through a 0.22- μm filter (Millipore, Burlington, MA, U.S.). For heat-killing of bacteria, 10^{10} CFUs of *S. lentus* were incubated in 10mL of PBS at 85 °C for 10 min.

22. Tape stripping of mouse skin

Back skin of P1 mice and shaved back skin of P14 mice were stripped with tape (D-squame 3.8 cm²; CuDerm, Dallas, Texas, U.S.) once. The tapes were stored at -80 °C.

23. Quantification of tryptophan metabolites

Quantification of tryptophan metabolites analysis was performed using UPLC (Waters UPLC system; Acquity) coupled with triple quadrupole mass spectrometry (TQ-MS; Xevo TQ-XS). Skin samples from tape stripping were extracted using 900 μL of methanol-water (1:9, v/v) and dried. The two samples were pooled and reconstituted using 1 mL of methanol-water (1:1, v/v) containing 5 nM tryptophan-d5. Separation was performed on a Scherzo SM-C18 column (1.7 μm \times 2.1 \times 100 mm). Mobile phases A and B were comprised of 0.2% formic acid in water and 0.2% formic acid in acetonitrile, respectively. Samples were eluted at 400 $\mu\text{L}/\text{min}$ for 10 min. The linear gradient elution was as follows: 0.0–2.0 min, 95% B; 4.0–6.0 min, 95%–65% B; 6.0–8.0 min, 100% B; 8.0–8.5 min, 100–95% B; 8.5–10.0 min, 95% B. MS/MS experiments were conducted in positive ion mode with the following parameters: capillary voltage of 2.0 kV, cone 13.0 V, source temperature 15 K, desolvation temperature 650 K, cone gas flow 150 L/h, collision gas flow 0.15 mL/min, nebulizer gas flow 7 bar. Quantification was performed in multiple reaction monitoring (MRM) mode and MRM transitions used in quantification of tryptophan metabolites. Individual tryptophan metabolite standards were used to optimize the condition of each metabolite, and a series of calibration solutions was prepared to generate calibration curves.

24. HaCaT cell culture

The human keratinocyte cell line HaCaT (RRID: CVCL_0038) was maintained in Dulbecco's modified eagle medium (DMEM, [Lonza]) with 10% fetal bovine serum (Gibco, Waltham, MA, U.S.) (FBS) and 1% antibiotics (10,000 µg/mL streptomycin and 10,000 U/mL penicillin [Gibco]) at 37 °C with 5% CO₂. Medium was replaced every other day with fresh medium. HaCaT cells were seeded in 12-well plates and cultured until they reached 80–90% confluence. After further cultivation for 24 h, cells were incubated with sterilely-filtered bacterial supernatants diluted in DMEM to 30% of the total volume at 37 °C in 5% CO₂ for another 2 h and 16 h. Cell were incubated for 2 h and 16 h with or without heat-killed *S. lentus* (bacteria:HaCaT cell ratio, 250:1). Cells were incubated with the same percentage of corresponding bacterial media (TSB) as the control. For treatment with tryptophan metabolite, cells were treated with different doses (0.3 mM–0.5 mM) of tryptophan metabolites (indole acetic acid; IAA and indole-3-aldehyde; IAld; Sigma-Aldrich) at 37 °C in 5% CO₂ and incubated for another 16 h. Cells were harvested for RNA collection. RNA from HaCaT cells was prepared using the RNeasy®Mini Kit (Qiagen) following the manufacturer's instructions. RNA was quantified by a NANODROP 1000 spectrophotometer; RNA (500 ng) was reverse transcribed using PrimeScript™ RT Master Mix according to the manufacturer's instructions. qPCR was conducted using QuantStudio 3 Real-Time PCR using KAPA SYBR® FAST ABI Prism®. We assessed the expression of *GAPDH* (NM_002046.7) and *TSLP* (NM_033035.5). Quantification of gene expression was determined by the comparative $2^{-\Delta\Delta CT}$ method. The relative expression levels were determined by normalizing expression to *GADPH*.

25. RNA isolation and quantitative polymer chain reaction

Total skin RNA from the MC903 model was prepared using RNeasy® Fibrous Tissue Mini Kit (Qiagen) following the manufacturer's instructions. RNA from KCs was prepared using RNeasy® Mini Kit (Qiagen) following the manufacturer's instructions. RNA was

quantified by NANODROP 1000 spectrophotometer (Thermo Fisher Scientific), and 500 ng was reverse transcribed using PrimeScript™ RT Master Mix (Takara, Kusatsu, Japan) according to the manufacturer's instructions. qPCR was conducted on QuantStudio 3 Real-Time PCR using KAPA SYBR® FAST ABI Prism®. We assessed gene expression: *Tslp* (NM_021367.2), *Il33* (NM_133775.3), *Hprt* (NM_013556.2), *Il7* (NM_008371.5), *Ccl20* (NM_016960.2, NM_001159738.1) and *Il18* (NM_001357221.1). Quantification of gene expression was determined by the comparative $2^{-\Delta\Delta CT}$ method. The relative expression levels were determined by normalizing expression to Hypoxanthine-guanine phosphor-ribosyltransferase (*Hprt*).

26. Quantification and statistical analysis

The data were analyzed by GraphPad Prism 8.0 software and are presented as means \pm SEM or SD as indicated. Two-tailed unpaired Student's *t*-tests were performed to determine statistical significance. $P < 0.05$ was considered significant.

III. RESULTS

1. AD-like skin inflammation is attenuated by constitutive deficiency of commensal microbiota

Previous studies have shown that topical application of MC903, a low-calcemic analog of vitamin D3 (calcipotriol) to mouse skin induces an AD-like dermatitis model recapitulated with features of inflammation, itch, and barrier dysfunction.^{40, 54-56} To explore the role of commensal microbiota in shaping AD-like inflammation, we first examined the degree of MC903-induced inflammation in GF mice compared with mice housed in specific pathogen-free (SPF) barrier conditions. GF mice showed significantly reduced ear swelling and histological inflammation as measured by total epidermal thickness and dermal inflammatory cell infiltration compared to SPF mice (Figure. 1A-C). Moreover, local gene expression of *Tslp* and *Il33*, typical markers for type 2 inflammation in MC903 model,^{40, 57-59} was decreased over day 5 and 7 in GF compared to SPF mice (Figure 1D). To understand the unbiased molecular differences in MC903-induced inflammation between SPF and GF conditions, RNA-sequencing was performed. AD-like inflammation in GF mice exhibited significantly different gene expression patterns compared to SPF mice (Figure 1E and F). Gene set enrichment analysis (GSEA) showed that the neuron developmental pathway associated with itch symptom in the AD-like MC903 model⁶⁰ was significantly enriched in SPF compared to GF conditions (Figure 2A). However, the keratinization pathway involved in the integrity of skin barrier function was significantly enriched in GF compared to SPF conditions (Figure 2A). To understand the global enrichment of type 2 immune responses, we performed gene set variation analysis (GSVA) using the representative type 2 immune signature gene sets. GSVA results demonstrated that, although type 2 immune signatures were largely increased in MC903-treated SPF mouse skins, MC903-treated GF mouse skins showed a generally decreased enrichment (Figure 1G). Previous studies have demonstrated that topical application of MC903 induces overexpression of TSLP from KCs, which promotes local ILC2 activation.^{40, 54, 61} To further understand the differential

involvement of skin ILC subsets in AD-like inflammation between SPF and GF conditions, we performed GSEA using the signature gene sets for skin ILCs (GSE180885).⁶² Interestingly, MC903-treated SPF mice showed a significantly increased enrichment of skin ILC2 signature compared to GF mice, however, no significant differences were found in ILC1 and ILC3 signatures (Figure 1H), suggesting that ILC2-mediated immunity is potentially reduced in AD-like inflammation of GF mice. To examine whether transient depletion of local microbiota affects AD-like inflammation, MC903 model was induced in SPF mice treated with topical or oral antibiotics (ABX) to disrupt the skin or gut microbiota, respectively. Notably, the severity and *Tslp* expression of AD-like inflammation were not reduced by transient disruption of the local microbiota (Figure 1I-O and 2B-E). Furthermore, conventionalization of GF mice to SPF conditions from birth rescued AD-like inflammation (Figure 2F-I). Collectively, these data indicate that the constitutive absence of commensal microbiome is associated with reduced AD-like inflammation.

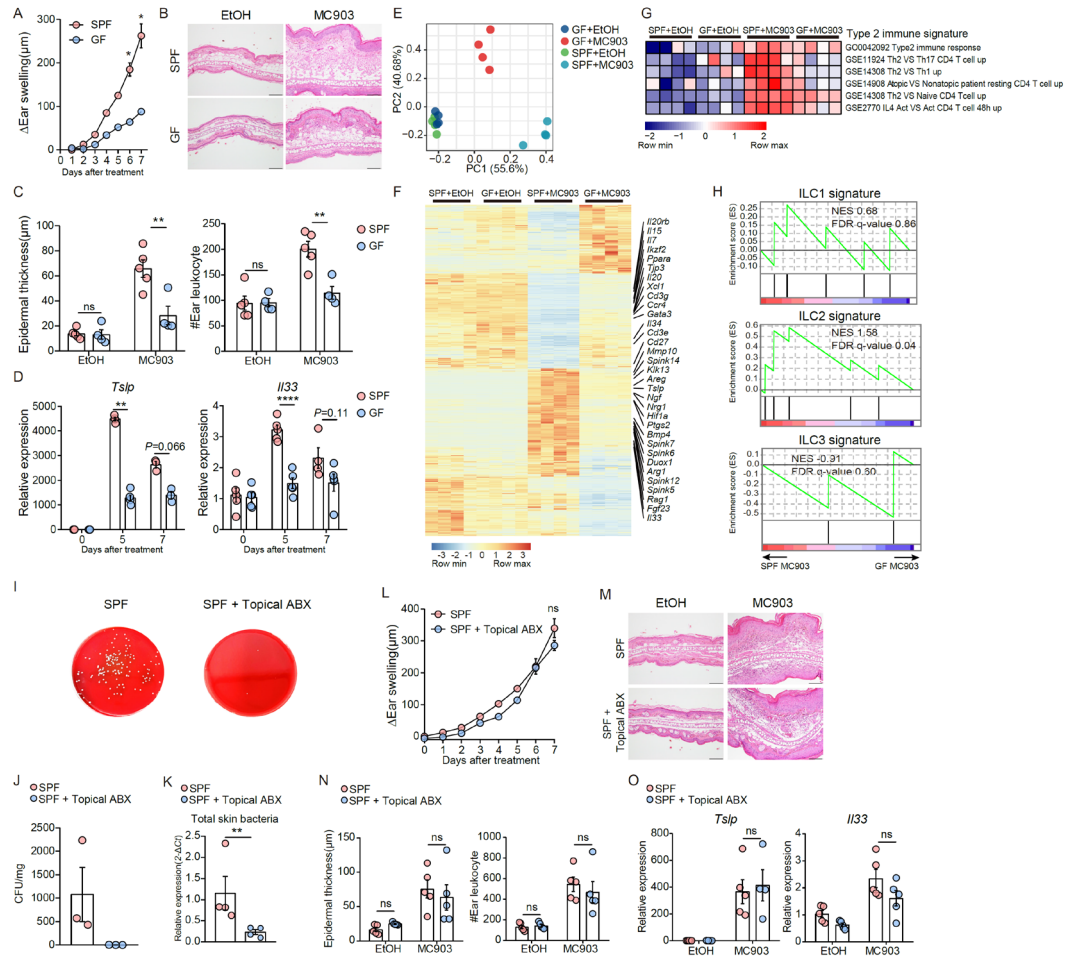


Figure 1. Commensal microbiota is responsible for pathophysiology in MC903-induced AD-like allergic skin inflammation. (A and B) Ear swelling (A) and H&E staining of ear skin (B) from daily ethanol (EtOH)- or MC903-treated SPF and GF mice (scale bars = 100 μm). (C) Epidermis thickness (left) and accumulated leukocyte number (right). (D) Gene expression in ear skin at indicated time points. (E and F) Principal component (PC) analysis (E) and heatmap (F) of whole skin gene expression. (G) Heatmap of gene set variation analysis using representative type 2 immune signature gene sets. (H) Gene set enrichment analysis of differentially expressed genes between MC903-treated

SPF and GF mouse skin. (I) Bacterial colonies from the skin homogenates of topical antibiotics (ABX)-treated (right) and untreated (left) SPF mice. (J and K) Colony-forming units (CFUs) of skin homogenates (J) and relative expression of 16S subunit in skin swab samples (K). (L and M) Ear swelling (L) and H&E staining of ear skin (M) from daily EtOH- or MC903-treated SPF mice with or without topical ABX treatment (scale bars = 100 μm). (N) Epidermis thickness (left) and accumulated leukocyte number (right). (O) Gene expression in ear skin of each group of mice. (A–D, I–O) Data are from one experiment representative of at least three independent experiments and displayed as mean \pm SEM; $n = 3\text{--}5$ mice per group and time point. * $P < 0.05$, ** $P < 0.01$, and **** $P < 0.0001$, and ns, not significant.

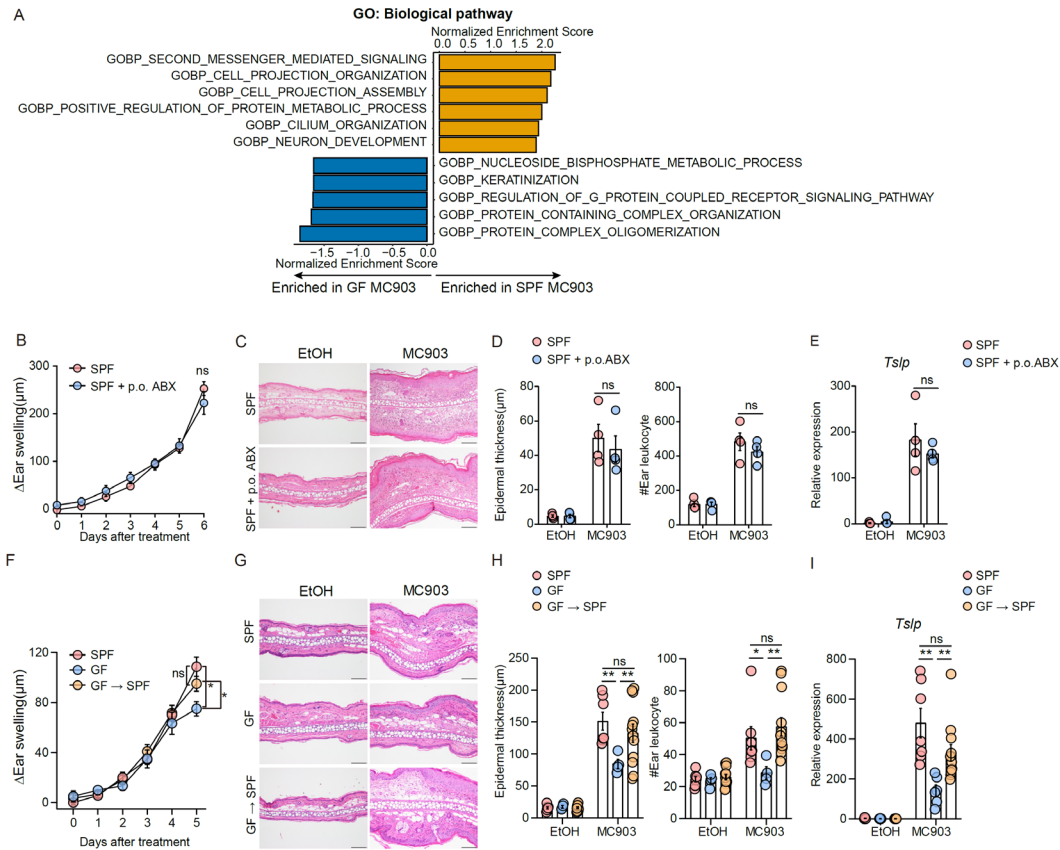


Figure 2. AD-like skin inflammation is attenuated by constitutive deficiency of commensal microbiota. (A) Gene set enrichment analysis of differentially expressed genes (\log_2 fold change ≥ 1.5 or ≤ -1.5) between MC903-treated SPF and GF mouse skins using gene sets for Gene ontology: Biological pathway (m5.go.bp.v2023.1.Mm.symbols.gmt). (B) Ear swelling response in daily MC903-treated SPF mice with or without oral antibiotics (p.o. ABX) treatment. (C) H&E staining of ear skin from daily EtOH- or MC903-treated SPF mice with or without ABX treatment (scale bars = 100 μm). (D) Epidermal thickness (left) and accumulated leukocyte number (right) from each group of mice. (E) *Tslp* gene expression in ear skin from each group of mice. (F) Ear swelling response in daily MC903-treated SPF, GF, and conventionalized GF (GF \rightarrow SPF) mice.

(G) H&E staining of ear skins from daily EtOH- or MC903-treated SPF, GF, and GF → SPF mice (scale bars = 100 μ m). (H) Epidermal thickness (left) and accumulated leukocyte number (right) from each group of mice. (I) *Ts/p* gene expression in ear skin from each group of mice. (B-I) Data are from one experiment representative of at least three independent experiments and displayed as mean \pm SEM; n = 4–12 mice per group and time point. ABX, antibiotics; EtOH, ethanol; GF, germ free; ns, not significant; p.o., per os; SPF, specific pathogen free. *P < 0.05 and **P < 0.01.

2. Microbiota colonization during specific neonatal window induces cutaneous ILC2 priming

Mounting evidence has revealed that the immune system undergoes dynamic maturation and imprinting during the postnatal life under the influence of microbiome.^{17, 63, 64} Since our data showed reduced severity of the MC903 model in conjunction with decreased ILC2 signatures in GF mice, but not transient microbial depletion in adults, we hypothesized that microbial exposure at distinct neonatal stages contributes to the threshold of AD-like inflammation by modulating early ILC priming as in the lung and intestine.⁶⁵⁻⁶⁸ To understand the unbiased developmental dynamics of postnatal skin ILCs, we performed single-cell RNA-sequencing (scRNA-seq) of total ILCs in mouse skin at postnatal day 1 (P1) and P14. Overall, ILC clusters were largely distinct between P1 and P14 skin (Figure 3A-D). *Tcf7⁺Pdcd1⁺* progenitor, *Mki67⁺* proliferating, and *Calca⁺* ILC populations in P1 skin were rapidly substituted by more committed ILC subsets by P14, including *Il18r1⁺* NK/ILC1s, *Il2ra⁺Pdcd1⁺* ILC2s, *Rorc⁺Ccr6⁺* ILC3s, and relatively undefined ILCs (indeterminate ILCs). In particular, we identified a distinct population of ILC2s confined to P14 skin that strongly expressed *Il5*, *Gata3*, *Areg*, *Il1rl1*, *Klrg1*, and *Il2ra* (Figure 3A-E), indicating their unique identity of fully mature ILC2s (primed ILC2s).⁶⁵ Pseudotime trajectory analysis revealed a continuous developmental pathway in which primed ILC2s arose through other ILC subsets, including ILC2s (Figure 3F). These results indicate that a highly dynamic transition of cutaneous ILCs into more committed subsets occurs during early postnatal window.

To assess the early neonatal development of primed ILCs fully competent to produce effector cytokines, we analyzed the kinetics of cytokine production by ILCs in SPF mouse skin following stimulation with phorbol myristate acetate (PMA) and ionomycin. A marked accumulation of ILCs was observed in neonatal skin as early as P3–P7, which was maintained through adulthood (Figure 3G and H). The frequency of IL-5⁺ ILC2s and IL-17A⁺ ILC3s was increased between P7–P14 and retained through P56 (Figure 3G and H).

To examine whether ILC expansion and/or priming during neonatal period was regulated by early commensal microbiota exposure, we compared the frequencies of ILCs between SPF and GF mouse skin at P14 and P56. Although the early expansion of ILCs was comparable between SPF and GF mice, the proportion of IL-5⁺ ILC2s was significantly reduced in GF mice both at P14 and P56, while that of IL-17A⁺ ILC3s did not differ (Figure 3I-L). The frequencies of CD25⁺ ILCs, T-bet⁺ ILC1s, GATA3⁺ ILC2s, and RORγt⁺ ILC3s, as well as Foxp3⁺ Tregs and GATA3⁺ Th2 cells, were largely comparable between SPF and GF mouse skin at both postnatal and adult stages, in part similar to previous studies (Figure 4A and B).^{13, 69} Moreover, transient depletion of the skin commensal microbiota by topical ABX treatment before P14, but not P56, significantly reduced the proportion of primed ILC2s (Figure 4C and D), further supporting the role of early microbial exposure in cutaneous ILC2 priming.

We further assessed the importance of early ILC2 priming in determining the extent of AD-like inflammation in adults. The severity of the MC903 model was not reduced in SPF *Rag1*^{-/-} mice (Figure 4E-H) and SPF wild-type (WT) mice treated with CD4-depleting antibodies (Figure 4I-L), indicating a redundant role for T cells as previously reported.⁴⁰ To test the functional role of postnatally primed ILC2s, we used an anti-CD25 monoclonal antibody to deplete ILC2s in P14 SPF *Rag1*^{-/-} mice^{40, 70} and induced the MC903 model in adults (Figure 4M). Notably, mice depleted with postnatal ILC2s showed a significantly attenuated AD-like inflammation in adulthood (Figure 4N-Q). In addition, Th2 cell immune responses of MC903-induced inflammation, potentially boosted by ILC2 activity,⁷¹⁻⁷³ were similar between SPF and GF mice (Figure 4R), supporting that the reduced AD-like inflammation observed in GF mice potentially results from inefficient postnatal ILC2 priming. Collectively, these data suggest that cutaneous ILC2 priming occurs during a specific neonatal period in response to commensal microbial exposure and persists into adulthood to participate in AD-like inflammation.

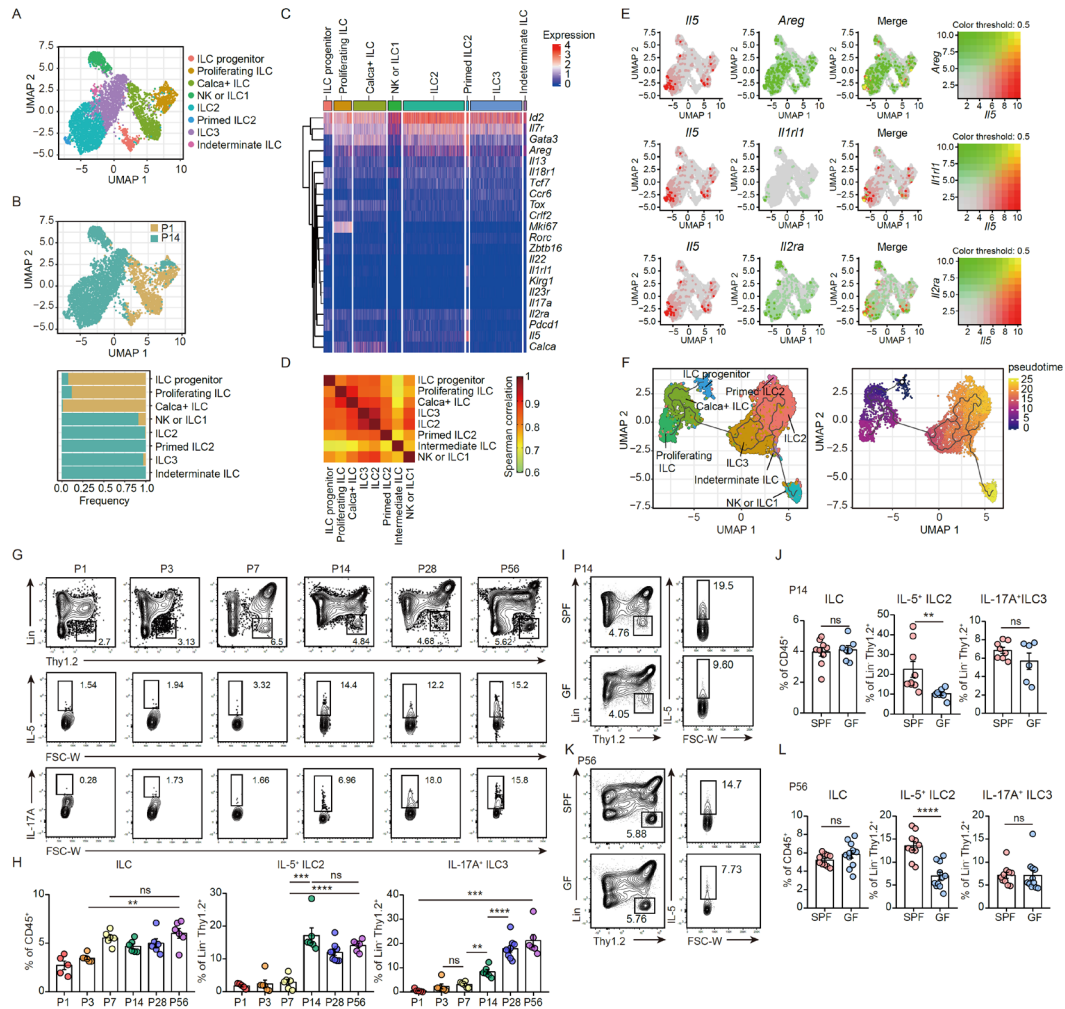


Figure 3. Microbiota colonization during specific neonatal window induces cutaneous ILC2 priming. (A-F) Single-cell RNA sequencing of total ILCs (CD45⁺Lin⁻Thy1.2⁺) sorted from mouse skin at postnatal day 1 (P1) and P14. (A and B) UMAP plot (A) and proportional plot (B) of ILC clusters. (C) Heatmap of selected genes to specify ILC subsets. (D) Correlation matrix for global gene expression. (E) UMAP plots for co-expression of *Il5* and indicated genes. (F) Pseudo-time trajectory analysis for early postnatal ILC clusters. (G and H) Representative flow cytometry plots (G) and bar graphs (H) for PMA/ionomycin

-stimulated ILCs in SPF mouse skin at indicated time points. (I-L) Representative flow cytometry plots (I and K) and bar graphs (J and L) for ILCs at P14 (I and J) and P56 (K and L) skin under SPF and GF conditions. (G-L) Data are from one experiment representative of at least three independent experiments and displayed as mean \pm SEM; $n = 5-11$ mice per group. $**P < 0.01$, $***P < 0.001$, and $****P < 0.0001$, and ns, not significant.

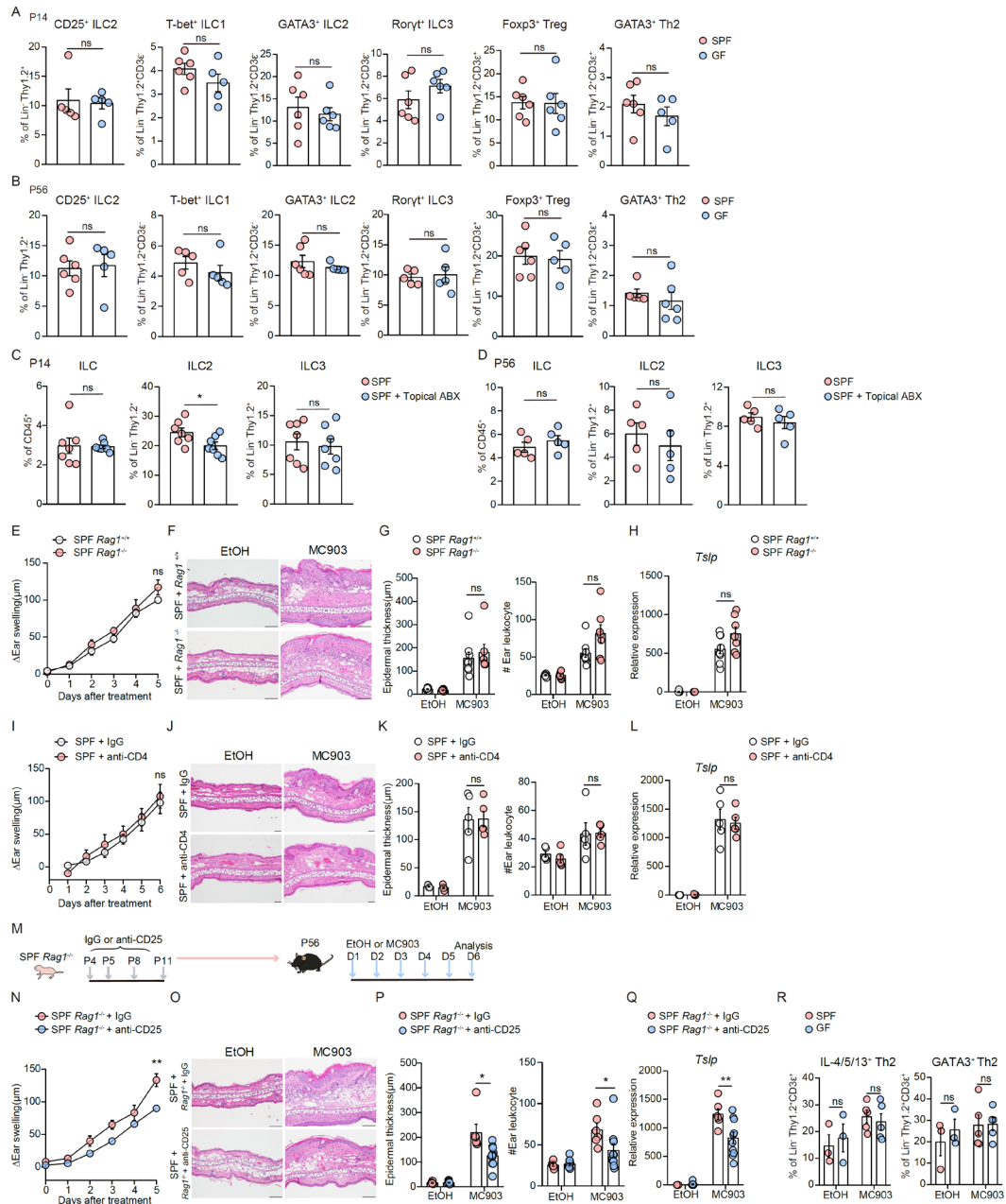


Figure 4. Cutaneous ILC2 priming during specific neonatal window is responsible for pathophysiology in MC903-induced AD-like allergic skin inflammation. (A and B)

CD25, T-bet, GATA3, and ROR γ t expression in innate lymphoid cells (ILCs; CD45⁺Lin⁻Thy1.2⁺), and FoxP3 and GATA3 expression in T cells (CD45⁺Lin⁻Thy1.2⁺ CD3 ϵ ⁺; Lin⁻ excepting CD3 ϵ) from postnatal day14 (P14) (A) and P56 (B) skin under SPF and GF conditions. (C and D) Proportion of total ILCs, IL-5⁺ ILC2s, and IL-17A⁺ ILC3s from P14 (C) and P56 (D) SPF mouse skin with or without topical antibiotic (ABX) treatment. (E) Ear swelling response in daily MC903-treated SPF *Rag1*^{+/+} or *Rag1*^{-/-} mice. (F) H&E staining of ear skins from daily EtOH- or MC903-treated SPF *Rag1*^{+/+} or *Rag1*^{-/-} mice (scale bars = 100 μ m). (G) Epidermal thickness (left) and accumulated leukocyte number (right) from each group of mice. (H) *Tslp* gene expression in ear skin from each group of mice. (I) Ear swelling response in daily MC903-treated SPF mice with anti-CD4 or isotype antibody treatment. (J) H&E staining of ear skins from daily EtOH- or MC903-treated SPF mice with anti-CD4 or isotype antibody treatment (scale bars = 50 μ m). (K) Epidermal thickness (left) and accumulated leukocyte number (right) from each group of mice. (L) *Tslp* gene expression in ear skin from each group of mice. (M) Experimental protocol for neonatal anti-CD25 antibody treatment and subsequent MC903-induced atopic dermatitis (AD)-like inflammation model in P56 SPF *Rag1*^{-/-} mice. (N) Ear swelling response in daily MC903-treated SPF *Rag1*^{-/-} mice after treatment with neonatal anti-CD25 or isotype antibodies. (O) H&E staining of ear skins from daily EtOH- or MC903-treated SPF *Rag1*^{-/-} mice after treatment with neonatal anti-CD25 or isotype antibodies (scale bars = 100 μ m). (P) Epidermal thickness (left) and accumulated leukocyte number (right) from each group of mice. (Q) *Tslp* gene expression in ear skin from each group of mice. (R) Expression of GATA3 and cytokines (IL-4, IL-5, IL-13) in T cells from P56 SPF and GF mouse skin with or without MC903 treatment for 5 days. (A-R) Data are from one experiment representative of at least three independent experiments and displayed as mean \pm SEM; n = 3–10 mice per group. ABX, antibiotics; EtOH, ethanol; GF, germ free; ILCs, innate lymphoid cells; ns, not significant; P, postnatal day; SPF, specific pathogen free; Th2, T helper 2 cells; Treg, regulatory T cells. *P < 0.05 and **P < 0.01.

3. Microbiota-induced TSLP production in keratinocytes is responsible for postnatal ILC2 priming

To investigate the underlying cues involved in postnatal ILC2 priming in association with microbiota, we first performed KEGG pathway analysis for genes upregulated in primed ILC2s compared to other ILC subsets obtained from scRNA-seq. We found that the JAK-STAT signaling pathway, which is mainly activated by cytokine-cytokine receptor interactions, was one of the highly enriched pathways in primed ILC2s (Figure 5A), and *Jak2* was highly expressed in this subset (Figure 5B). At the forefront of bacteria-skin interface, KCs interact closely with commensal microbiota to maintain functional barrier homeostasis.^{17, 74} To understand the KC-derived factors that may affect postnatal ILC2 priming (Figure 5C), we investigated gene expression profiles of early postnatal KCs and performed KEGG pathway analysis for genes upregulated in P14 compared to P1 KCs. KCs demonstrated dynamic changes in gene expression during the first two weeks of postnatal period (Figure 5D and E). We found that the cytokine-cytokine receptor interaction pathway consisting of several cytokines, such as IL-7, BMP4, BMP3, IL-33, and TSLP, was the most enriched pathway in P14 KCs (Figure 5F). Among the upregulated cytokines in KCs throughout P1-P14 (Figure 5G and 6A), IL-7 and TSLP are known to activate the downstream JAK-STAT signaling pathway,^{75, 76} suggesting that IL-7 and TSLP could be potentially involved in JAK-STAT signal activation in postnatal primed ILC2s. We next assessed whether the expression levels of these cytokines are influenced by commensal microbiota. Notably, the expression of *Tslp*, but not *Il7*, was significantly decreased in GF compared to SPF KCs at P14 and P56 (Figure 5H and I). Moreover, transient depletion of the skin commensal microbiota by topical ABX treatment before P14 also significantly reduced the expression levels of *Tslp*, but not *Il7* (Figure 6B), suggesting that colonization of the skin microbiota actively induces early postnatal *Tslp* expression in KCs, which is maintained into adulthood.

To investigate whether TSLP mediates ILC2 priming in early neonates, we examined the proportion of ILC subsets in the skin of P14 SPF mice treated with receptor-blocking or cytokine-neutralizing antibodies. Similar to previous reports,⁶¹ development of cutaneous ILCs was significantly disrupted by blockade of IL-7R α , a shared receptor subunit of TSLP and IL-7 (Figure 6C and D), and neutralization of IL-7 also significantly reduced ILC frequency without affecting priming of ILC2s and ILC3s (Figure 5J and K). However, neutralization of TSLP significantly reduced the proportion of IL-5⁺ ILC2s, but not total ILCs or IL-17A⁺ ILC3s (Figure 5L and M). Similarly, the frequency of IL-5⁺ ILC2s was also diminished in *Tslp*-deficient mice at P14 compared with WT littermates (Figure 5N and O, 6E), suggesting that skin microbiota-dependent TSLP induction is responsible for postnatal ILC2 priming. Previous studies have demonstrated that ILC2s in the skin express IL-18R α , and IL-18 signaling is required for IL-5 production.⁶⁹ Although *Il18* expression was induced throughout P1-P14 in postnatal SPF KCs (Figure 6F), its expression level did not differ between SPF vs GF P14 KCs (Figure 6G). In addition, either SPF or GF P14 ILC2s expressed similar levels of IL-18R α (Figure 6H and I) and early postnatal ILC2 priming was limited by blockade of IL-18R α signaling (Figure 6J).

Previous studies have shown that postnatal colonization of the gut commensal bacteria upregulates epithelial expression of CCL20, which activates CCR6⁺ lymphoid tissue inducer cells, one of the intestinal ILC3 subsets.⁷⁷ Although the level of *Ccl20* was increased in KCs from P1 to P14 (Figure 5E and G, 6A), its expression between SPF and GF KCs was similar at P14 (Figure 5H), and topical ABX treatment before P14 was insufficient to reduce the expression of *Ccl20* in KCs (Figure 6B). However, P56 GF KCs showed reduced expression of *Ccl20* compared to SPF KCs (Figure 5I), suggesting that *Ccl20* expression in adult skin, but not postnatal skin, is likely influenced by skin microbiota. Moreover, FACS analyses showed that, although overall frequency of ILC3s between SPF and GF mouse skin was comparable (Figure 3I-L), P14 ILC3s was decreased in *Ccr6*^{-/-} compared with WT mice (Figure 6K and L).

Taken together, these data suggest that TSLP in KCs is responsible for postnatal ILC2

maturation and priming in a skin microbiota-dependent manner, whereas IL-18 and CCL20/CCR6 induce ILC2 and ILC3 priming, respectively, in a skin microbiota-independent manner.

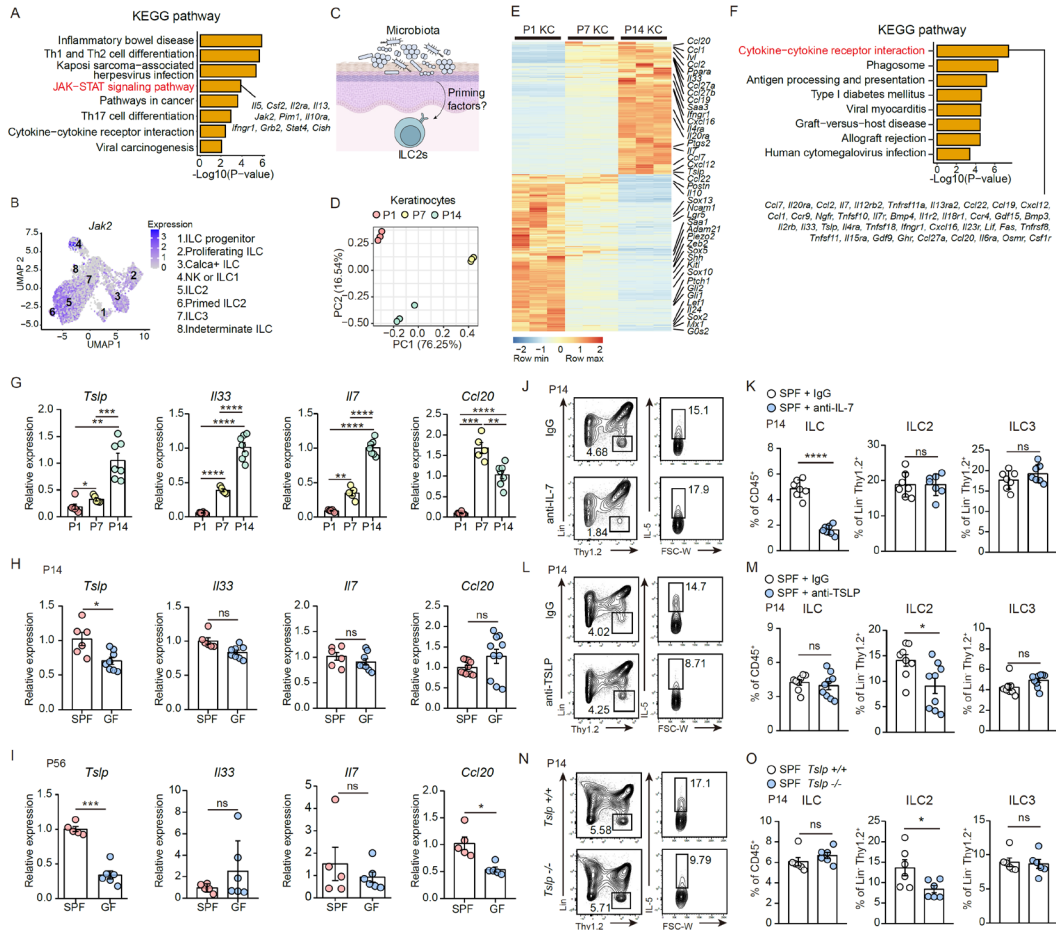


Figure 5. Microbiota-induced TSLP production in keratinocytes is responsible for postnatal ILC2 priming. (A) KEGG pathway analysis of genes upregulated in primed ILC2s. (B) UMAP plot for *Jak2* expression in ILC subsets. (C) Schematic illustration of microbiota-dependent keratinocyte (KC)-derived factors affecting ILC2 priming. (D-E) Principal component (PC) analysis (D) and heatmap (E) of gene expression in sorted KCs from postnatal day 1 (P1), P7, and P14 SPF mice. (F) KEGG pathway analysis of genes upregulated in P14 vs P1 KCs. (G) Expression levels of indicated genes from sorted KCs from SPF mice. (H and I) Gene expression of sorted KCs between SPF and GF mice at P14 (H) and P56 (I). (J-M) Representative flow cytometry plots and bar graphs of P14 skin

ILCs after treatment with anti-IL-7 (J and K) and anti-TSLP (L and M) antibodies. (N and O) Representative flow cytometry plots (N) and bar graphs (O) of P14 skin ILCs between SPF *Tslp*^{+/+} and *Tslp*^{-/-} mice. (D and E) Each RNA-sequencing sample comprised pooled KCs from 2–3 mice. (G–O) Data are from one experiment representative of at least three independent experiments and displayed as mean \pm SEM; n = 5–10 mice per group. *P < 0.05, **P < 0.01, ***P < 0.001, and ****P < 0.0001, and ns, not significant.

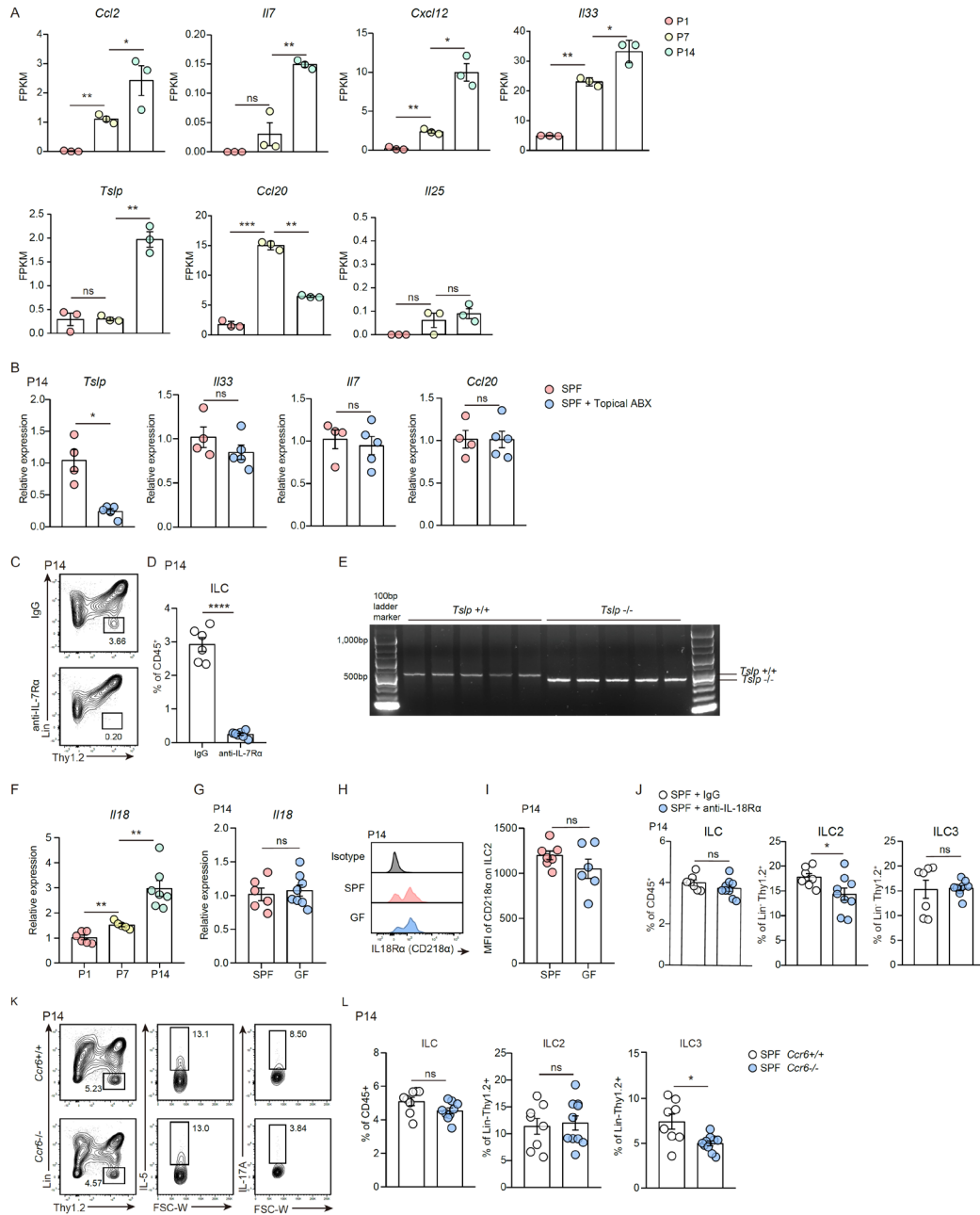


Figure 6. TSLP in KCs is responsible for postnatal ILC2 maturation and priming in a skin microbiota-dependent manner, whereas IL-18 and CCL20/CCR6 induce

ILC2 and ILC3 priming in a skin microbiota-independent manner. (A) FPKM of indicated genes from sorted keratinocytes (KCs) from postnatal day 1 (P1), P7, and P14 SPF mouse skin. (B) Expression levels of indicated genes from sorted KCs from P14 SPF mice with or without topical antibiotics (ABX) treatment. (C and D) Representative flow cytometry plots (C) and bar graphs (D) of P14 skin total ILCs (CD45⁺Lin⁻Thy1.2⁺) after treatment with anti-IL-7R α or isotype antibodies. (E) Genotyping of *Tslp*^{+/+} and *Tslp*^{-/-} mice. Primers amplified ~0.5 Kb fragments of the wild-type allele and ~0.4 Kb fragments of the knockout allele. (F) *Il18* expression of sorted KCs from P1, P7 and P14 in SPF mouse skin. (G) *Il18* expression of sorted KCs from P14 skin under SPF and GF conditions. (H and I) Histogram (H) and graph for the mean fluorescence intensity (MFI) (I) of IL-18R α from P14 skin IL-5⁺ ILC2s under SPF and GF conditions. (J) Proportion of total ILCs, IL-5⁺ ILC2s, and IL-17A⁺ ILC3s P14 SPF mouse skin treated with anti-IL-18R α or isotype antibodies. (K and L) Representative flow cytometry plots (K) and bar graphs (L) of total ILCs, IL-5⁺ ILC2s, and IL-17A⁺ ILC3s from P14 SPF *Ccr6*^{+/+} or *Ccr6*^{-/-} mouse skin. (A) Each RNA-seq KC sample was pooled from 2–3 mice. (B, F, G) Sorted KC samples were pooled from 2–3 individual mice. (C-E, H-L) Data are from one experiment representative of at least three independent experiments and displayed as mean \pm SEM; n = 5–10 mice per group. ABX, antibiotics; GF, germ free; ILCs, innate lymphoid cells; KCs, keratinocytes; ns, not significant; P, postnatal day; SPF, specific pathogen free. *P < 0.05, **P < 0.01, ***P < 0.001, and ****P < 0.0001.

4. The early postnatal skin commensal microbe *Staphylococcus lentus* sufficiently induces TSLP production and ILC2 priming

To investigate the skin commensal microbes responsible for TSLP induction, we analyzed the skin microflora of SPF mice from early life to adulthood through full-length 16S rRNA-sequencing of skin swabs. Full-length 16S rRNA-sequencing revealed higher coverage of taxa assignment in comparison to partial fragments sequencing (Figure 8A). Comparison of microbial composition between whole-body and ear skin showed similar profiles, suggesting that the whole-body skin microbiome could represent the microbial community profile of ear skin (Figure 8B). Furthermore, sequencing of mock communities and negative control samples revealed reliable and accurate 16S rRNA-sequencing data obtained in our hands (Figure 8C-E). Throughout the postnatal period, skin showed highly dynamic colonization with commensal microbial communities (Figure 7A). Interestingly, principal coordinates analysis (PCoA) revealed rather similar compositions of skin commensal bacteria between P7, P14, and P21, which are distinct from the P28 and P56 stages (Figure 7B), suggesting the importance of weaning as reported in the gut immune system⁷⁸ or physiological changes of the skin⁷⁹ in regulating skin commensalism. Previous studies have shown that distinct species of *Staphylococcus* actively regulate skin immune responses by modulating IL-17A⁺CD8⁺ T cells or ILC3s in adults,^{13, 80} but their potential contribution to early postnatal ILC priming has not been determined. Considering that *Staphylococcus* was one of the dominant skin commensal bacteria during P7-P14 when ILC2 priming occurs (Figure 7A), we analyzed the kinetics of compositional changes of *Staphylococcus* at the species level. In the early postnatal period (P7, P14, and P21), we found that a distinct Staphylococcal species, *Staphylococcus lentus* (*S. lentus*), was the major Staphylococcal species, which was replaced by *Staphylococcus xylosum* (*S. xylosum*) in adulthood, a known skin commensal of adult laboratory mice (Figure 7C).^{14, 81} The existence of *S. lentus* was confirmed by culturing skin microbiota of SPF mice, and performing phylogenetic analysis of its genome, along with other *Staphylococcus* species

(Figure 8F). The *S. lentus* isolate was tightly bound to the representative *S. lentus* strain (bootstrapping value = 1). Moreover, multiple sequence alignment focusing on the V3-V4 region of the full-length 16S rRNA gene demonstrated a clear separation of *S. lentus* from other Staphylococcal species with an identity range of 96.6-96.8% (Figure 8G and H), suggesting the distinct identity of *S. lentus*. To investigate whether *S. lentus* directly induces *Tslp* expression in postnatal skin, GF mice were mono-associated with *S. lentus* isolates by consecutive topical application from P5 and gene expression was measured at P14. The expression level of *Tslp* in KCs increased after *S. lentus* exposure, whereas gene expression of *Il33* and *Il7* was not affected (Figure 7D). In line with *Tslp* induction, exposure to *S. lentus* significantly enhanced the proportion of IL-5⁺ ILC2s, but not overall ILCs or IL-17A⁺ ILC3s (Figure 7E). Furthermore, *Il18* expression in KCs was not induced by early exposure to *S. lentus* in GF mice (Figure 8I), further supporting the microbial independent role of IL-18 in early ILC2 priming. Thus, these data suggest that early postnatal colonization of *S. lentus* sufficiently induces local *Tslp* expression and ILC2 priming.

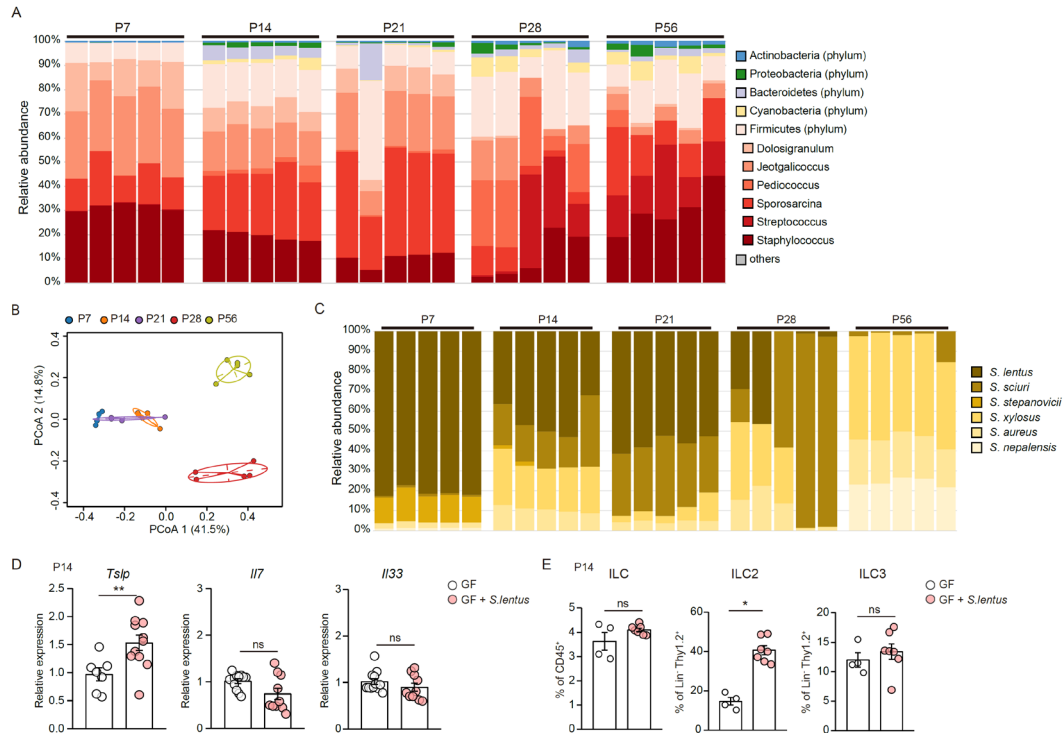


Figure 7. Early postnatal skin commensal microbe *Staphylococcus lentus* sufficiently induces TSLP production and ILC2 priming. (A) Relative abundance of major taxa based on 16S rRNA sequencing of postnatal day 7 (P7), P14, P21, P28, and P56 SPF mouse skin. (B) Principal coordinates analysis (PCoA) of 16S rRNA sequencing of skin swab samples. (C) Relative abundance of *Staphylococcus* species. (D and E) Gene expression of sorted keratinocytes (D) and proportion of total ILCs, IL-5⁺ ILC2s, and IL-17A⁺ ILC3s (E) from P14 GF mouse skin with or without topical association with *Staphylococcus lentus*. The GF control sample in (E) is identical to the GF control sample in Figure 9K because the experiment was performed simultaneously with the same control group. (A-C) Representative data from two independent experiments. (D and E) Data are from one experiment representative of at least three independent experiments and displayed as mean \pm SEM; $n = 4-11$ mice per group. * $P < 0.05$, ** $P < 0.01$, and ns, not significant.

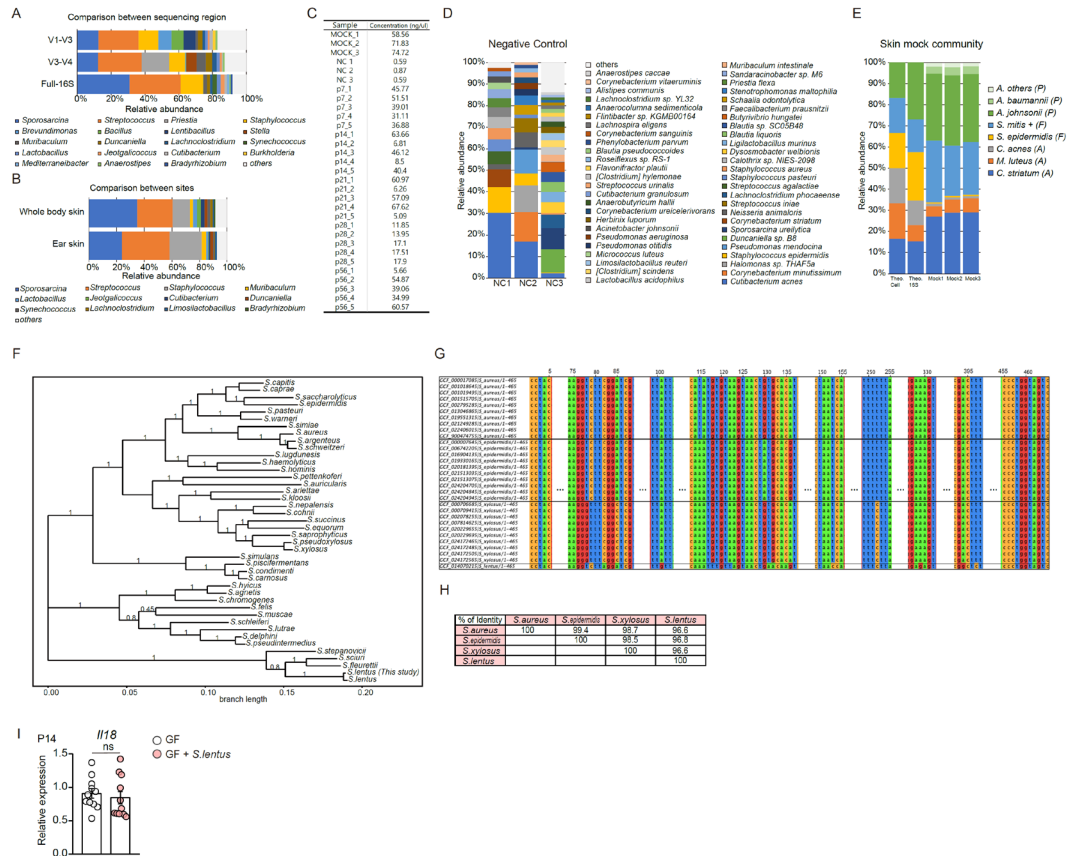


Figure 8. Clearly distinct skin commensal microbiote *Staphylococcus lentus* induces TSLP production and ILC2 priming during specific neonatal window. (A) Comparison of 16S rRNA sequencing among different regions (V1-V3, V3-V4, and 16S full-length) from skin swab samples of postnatal day 56 (P56) SPF mouse skin. (B) Comparison of 16S rRNA sequencing from swab samples between whole body and ear skin of P56 SPF mice. (C) Quantity of extracted microbiota DNA from skin mock community, negative controls, and P7, P14, P21, P28 and P56 SPF mouse skin. (D) Relative abundance of bacterial species from negative controls based on 16S rRNA sequencing. (E) Relative abundance of bacterial species from skin mock community based on 16S rRNA sequencing. (F) Relative abundance of major taxa based on 16S rRNA sequencing of postnatal day 7 (P7), P14, P21,

P28, and P56 SPF mouse skin. (G) Phylogenetic tree of *Staphylococcus* species including *S. lentus* isolates in this study. (H) Multiple sequence alignment (MSA) between *Staphylococcus aureus* (*S. aureus*), *Staphylococcus epidermidis* (*S. epidermidis*), *Staphylococcus xylosum* (*S. xylosum*), and *Staphylococcus lentus* (*S. lentus*). (I) Percentage of identity between *S. aureus*, *S. epidermidis*, *S. xylosum*, and *S. lentus*. (J) *Ill18* expression of sorted keratinocytes from P14 GF mouse skin with or without topical association with *S. lentus* four times prior to analysis. (A) Data are from one experiment. $n = 2-5$ mice per group. (B) Data are from one experiment. $n = 2$ mice per group. (C-F) Data are from one experiment representative of at least two independent experiments. $n = 5$ mice per group. (J) Sorted keratinocyte samples were pooled from 2-3 mice. Data are from one experiment representative of at least three independent experiments and displayed as mean \pm SEM; $n = 4-11$ mice per group, pooled from two independent experiments. GF, germ free; NC, negative control; ns, not significant; P, postnatal day; SPF, Specific pathogen free.

5. Tryptophan metabolite IAld-producing Staphylococcal species induce postnatal TSLP production and ILC2 priming

We asked how *S. lentus* colonization promotes postnatal TSLP induction and ILC2 priming. Expression of *TSLP* in HaCaT cells, an immortalized human keratinocyte cell line, was increased by treatment with *S. lentus* culture supernatant, but not with heat-killed *S. lentus*, suggesting that *S. lentus*-derived soluble factors (e.g., metabolites) are responsible for inducing *TSLP* in KCs (Figure 9A). Given the ability of microbial metabolites, especially Trp derivatives, to shape multiple immune cell development and function,^{33, 82} we hypothesized that *S. lentus*-derived metabolites are responsible for inducing neonatal TSLP expression and ILC2 priming. Genomic and metagenomic analyses revealed that the entire set of enzymes involved in Trp metabolism to produce indole acetic acid (IAA) were predicted to be produced by *Staphylococcus* species abundant in postnatal P7-P14 skin (Figure 10A). Therefore, we further analyzed the specific metabolic pathway-related genes required to catalyze Trp-derived metabolites (Figure 9B). We found that genes involved in the major IAld-generating Trp metabolic pathway (i.e., indole propionic acid (IPyA) route encompassing $\text{Trp} \rightarrow \text{IPyA} \rightarrow \text{IAA} \rightarrow \text{IAld}$), including aromatic amino acid aminotransferase (ArAT) (K00841), K04103, and K00128 (Figure 9B), were only observed in *Staphylococcus* species compared to other bacterial species that predominated in P7-P14 skin (Figure 9C). Furthermore, IAld-generating Trp metabolic pathway genes were highly conserved across multiple *Staphylococcus* species including *S. lentus* isolates (Figure 9D), suggesting that Staphylococcal species share a unique Trp metabolic pathway for IAld production. We next analyzed Trp metabolites of SPF mouse skin at P1 and P14 using LC/MS/MS analysis. Concentration of IAld, the end-product of the IAld-generating IPyA pathway, was significantly higher in P14 than in P1 skin (Figure 9E). To examine whether the Trp metabolites, IAA or IAld, are required for TSLP induction, we treated HaCaT cells with each metabolite and measured *TSLP* expression. IAld, but not IAA, significantly induced *TSLP* expression in a dose-dependent manner (Figure 9F). Indeed, consecutive

topical application of IAld from P5 GF mouse skin significantly induced local *Tslp* expression at P14 (Figure 9G). Importantly, exposure to IAld during the early postnatal period was sufficient to promote the emergence of IL-5⁺ ILC2s, but not total ILCs or IL-17A⁺ ILC3s (Figure 9H and I). As IAld-producing Trp metabolic pathway is conserved across Staphylococcal species (Figure 9D), we next explored whether other *Staphylococcus* species are also able to induce *Tslp* and early ILC2 priming. The expression of *Tslp* in P14 GF mouse KCs was significantly augmented by exposure to *S. xylosus* or *S. epidermidis*, which was accompanied by an increased proportion of IL-5⁺ ILC2s (Figure 9J and K). To directly examine the importance of IAld-producing Trp metabolic pathway in *Staphylococcus* for early ILC2 priming, we generated mutant strain for *S. aureus* deficient in ArAT (*S. aureus* Δ ArAT) (Figure 10B and C), a key enzyme for the major IAld-producing Trp metabolic pathway involving IPyA route. Notably, we found that GF mice with early postnatal exposure to WT *S. aureus* strain showed increased *Tslp* expression and ILC2 priming, but these effects were greatly reduced in GF mice exposed to the mutant *S. aureus* Δ ArAT strain (Figure 9L and M). Collectively, these data suggest that early postnatal colonization with specific IAld-producing Staphylococcal species including *S. lentus* actively promotes TSLP induction and ILC2 priming *in vivo*.

IAAId, indole-3-acetaldehyde; IAA, indole-3-acetic acid; IAId, indole-3-aldehyde). (C) Presence of IAA metabolic pathway-related genes in bacteria species. (D) Presence of IAA pathway-related genes in *Staphylococcus* species. (E) LC/MS/MS of Trp and Trp metabolites in skin tape strips from postnatal day 1 (P1) and P14 SPF mice. (F) *TSLP* expression in HaCaT KCs treated with Trp metabolites. (G) *Tslp* expression of sorted KCs from P14 GF mice with or without topical IAId treatment. (H and I) Representative flow cytometry plots (H) and bar graphs (I) for total ILCs, IL-5⁺ ILC2s, and IL-17A⁺ ILC3s from P14 GF mouse skin treated with ethanol (EtOH) or IAId. (J and K) *Tslp* expression of sorted KCs (J) and proportion of indicated ILC subsets (K) from P14 GF mouse skin with or without topical association with *Staphylococcus xylosus* (*S. xylosus*) or *Staphylococcus epidermidis* (*S. epidermidis*). (L and M) *Tslp* expression of sorted KCs (L) and proportion of indicated ILC subsets (M) from P14 GF mouse skin mono-associated with wild-type (WT) *Staphylococcus aureus* (*S. aureus* WT) or *S. aureus* Δ *ArAT* mutant. (A and F) Data are from one experiment representative of at least three independent experiments and displayed as mean \pm SD. (E) Data are from one experiment representative of two independent experiments; $n = 6-8$ mice per group. (G-K) Data are from one experiment representative of at least three independent experiments; $n = 4-15$ mice per group. (L and M) Data are pooled from two independent experiments and displayed as mean \pm SEM; $n = 4-16$ mice per group. * $P < 0.05$, ** $P < 0.01$, *** $P < 0.001$, and **** $P < 0.0001$, and ns, not significant.

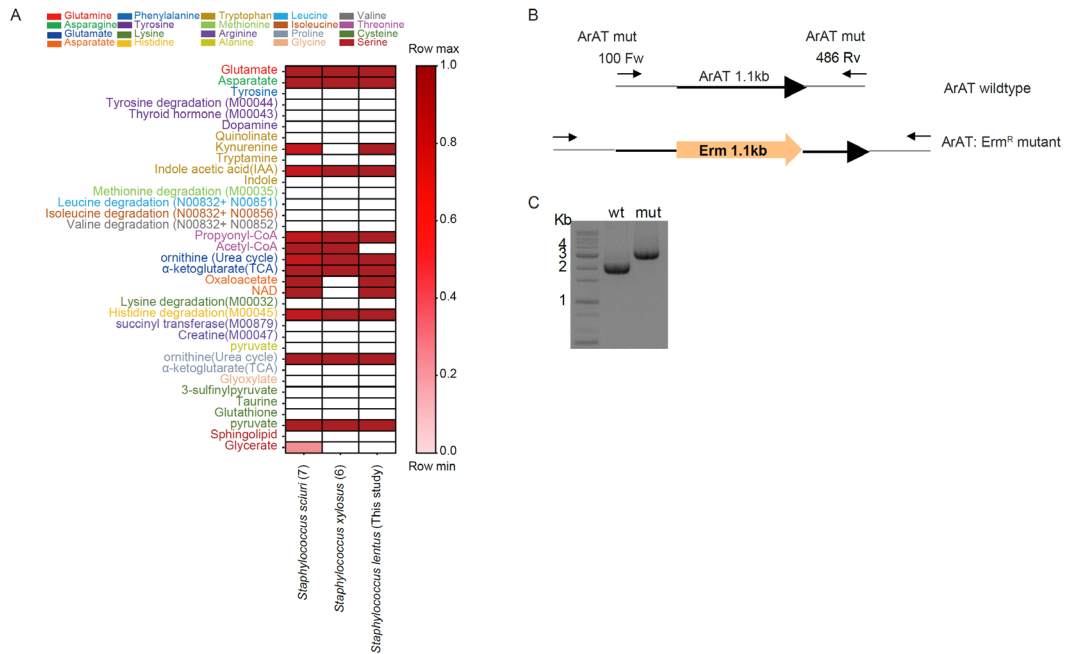


Figure 10. Amino acid metabolism-related genes in Staphylococcal species and mutant strain for *S. aureus* deficient in ArAT. (A) Presence of amino acid metabolism-related genes in representative *Staphylococcus* species found in postnatal day 7 (P7)-P14 SPF mouse skin. (B) Gene-targeting strategy for *Staphylococcus aureus* (*S. aureus*) Δ ArAT strain. (C) Genotyping of *S. aureus* wild type and Δ ArAT mutant strain. ArAT mutant primers amplified ~2 Kb fragments from the wild-type and ~3 Kb fragments from the mutant. ArAT, aromatic amino acid aminotransferase; mut, mutant; SPF, Specific pathogen free; WT, wild type.

6. Early postnatal *S. lentus*-TSLP-ILC2 priming axis is co-opted in AD-like inflammation in adults

We next investigated whether the timing of postnatal exposure to commensal *Staphylococcus* is responsible for promoting AD-like inflammation in adulthood. We exposed GF mice with *S. lentus* during early (P5-P11) or late (P28-P34) postnatal life and assessed the severity of MC903-induced model in P56 (Figure 11A). We found that early, but not late, exposure to *S. lentus* resulted in persistent induction of *Tslp* expression in KCs and increased frequency of primed ILC2s in adult P56 gnotobiotic mice (Figure 11B and C), consistent with the insufficient effect of transient depletion of commensal bacteria by topical ABX treatment in reducing primed ILC2s in adult mice (Figure 4D), despite efficient reduction of *S. lentus* in the skin (Figure 12A). In line with this, the severity of MC903-induced inflammation was correspondingly exacerbated in early exposed GF mice compared to the late exposed group (Figure 11D-G). Since early exposure to IAld induced postnatal *Tslp* expression and ILC2 priming at P14 (Figure 9G-I), we next examined whether early exposure to IAld is sufficient to facilitate AD-like inflammation in adults (Figure 12B). Surprisingly, GF mice early exposed to IAld did not show increased *Tslp* expression in KCs and frequency of primed ILC2s at P56 skin (Figure 12C and D). Furthermore, AD-like inflammation in adulthood was not exacerbated by early application of IAld (Figure 12E-G), indicating that IAld itself is not sufficient to maintain *Tslp* expression and primed ILC2s in adults. These results prompted us to test whether subsequent colonization with *S. lentus* is required to maintain the postnatal priming effect of ILC2s induced by early IAld exposure (Figure 11H). Notably, early IAld exposure followed by colonization of *S. lentus* in GF mice significantly promoted MC903-induced inflammation (Figure 11I-L), suggesting that sustained colonization of the commensal *Staphylococcus* after the early postnatal ILC2 priming period is required to maintain the priming effect of ILC2s. To directly examine the importance of IAld production in *Staphylococcus* in promoting AD-like inflammation later in life, GF mice were early

colonized with WT or $\Delta ArAT$ mutant *S. aureus* and the severity of MC903 model was assessed in adulthood (Figure 11M). GF mice with early exposure to *S. aureus* $\Delta ArAT$ strain showed significantly lesser degrees of AD-like inflammation than mice colonized with WT *S. aureus* (Figure 11N-Q). Previous studies have shown that *Escherichia coli* (*E. coli*) catalyzes Trp to indole via tryptophanase, a pathway different from the IAld-generating IPyA route.^{28, 83} Through genome comparison, we found that *E. coli* was devoid of a set of enzymes required for IAld catabolism compared to the representative *Staphylococcus* species, *S. xylosus* (Figure 12H). Interestingly, GF mice mono-associated with *S. xylosus* exhibited increased MC903-induced inflammation in adulthood, but this effect was not observed in GF mice early exposed to *E. coli* (Figure 12I-K), further supporting bacterial unicity for IAld-producing potential leading to predisposition to AD-like inflammation.

Finally, we asked whether skin microbiota-dependent early TSLP-ILC2 priming axis directly contributes to the AD-like inflammation in adults. ILCs isolated from P14 neonatal skin of GF WT, SPF WT, and SPF *Tslp*^{-/-} mice were adoptively transferred into recipient P56 GF mice via intradermal injection, and subsequently the severity of MC903-induced inflammation was assessed (Figure 13A). Intravital imaging showed that the transferred ILCs located around hair follicles and interfollicular areas, indicating successful engraftment (Figure 14A and B). GF mice transferred with P14 ILCs from SPF WT mice showed exacerbated MC903-induced inflammation compared to the GF WT ILC transplant group (Figure 13B-E). However, transfer of P14 ILCs from SPF *Tslp*^{-/-} mice did not promote AD-like inflammation (Figure 13B-E), suggesting that TSLP-dependent ILC2 priming in early postnatal period contributes to AD-like inflammation in adult recipients. In addition, frequencies of endogenous ILC2s and Th2 cells in recipient mice were not affected by transfer of P14 ILCs from SPF WT mice, regardless of MC903 treatment (Figure 14C and D), indicating that the predisposing effect on AD-like inflammation is mainly mediated by the activity of transferred ILCs. Furthermore, GF mice transferred with normalized numbers of primed ILC2s from GF donors relative to SPF donors exhibited similar degrees of AD-like inflammation compared to GF mice receiving SPF skin ILCs

(Figure 14E-H), supporting that different extent of postnatal ILC2 priming between SPF and GF skin leads to different severity of AD-like inflammation. Taken together, these data suggest that the early postnatal skin microbiota-TSLP-ILC2 priming axis promotes predisposition to AD-like inflammation later in life (Figure 15).

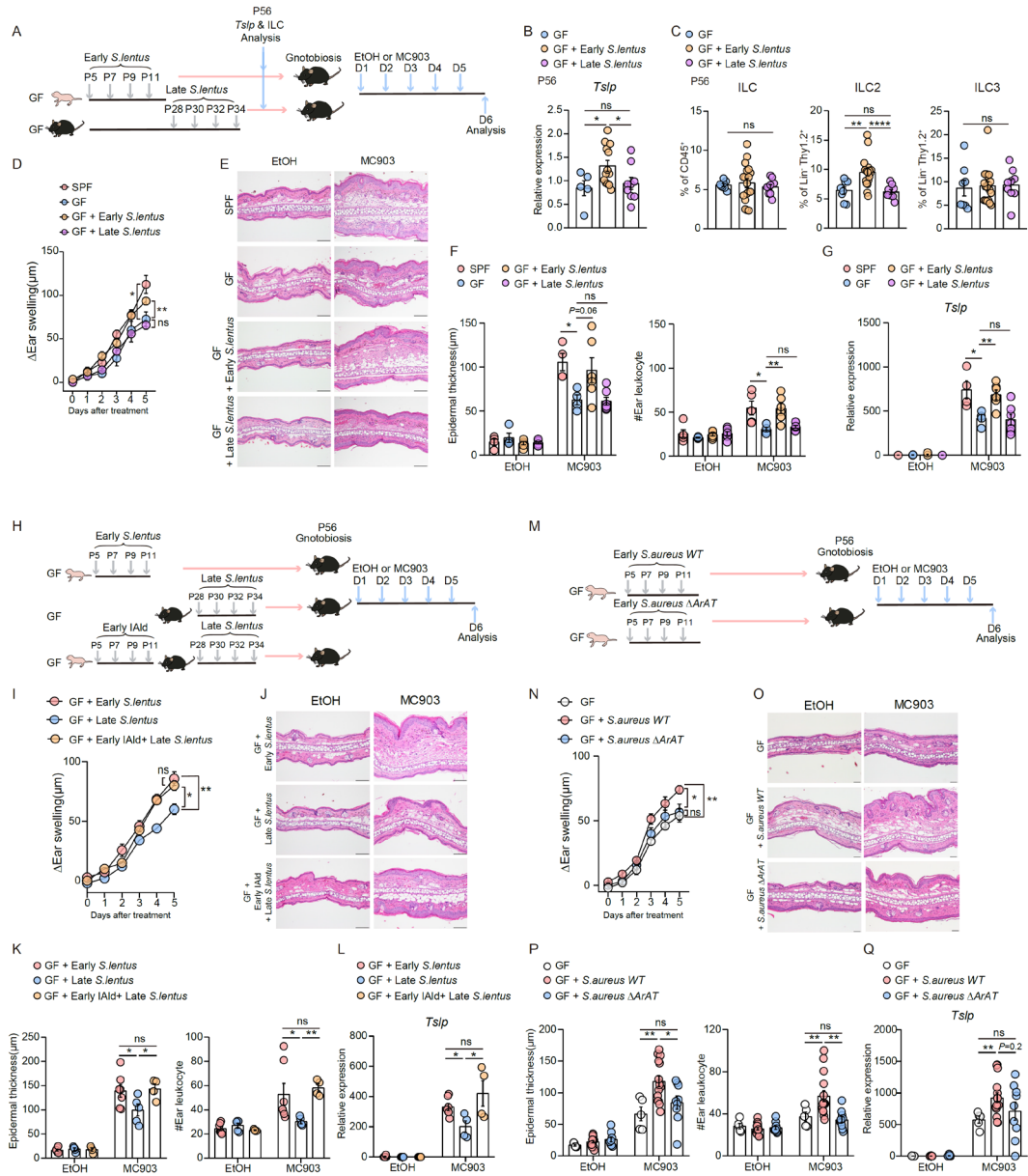


Figure 11. Early postnatal *S. lentus*-TSLP-ILC2 priming axis is co-opted in AD-like inflammation in adults. (A) Experimental scheme for mono-association of *Staphylococcus lentus* (*S. lentus*) and subsequent MC903-induced model. (B and C) *Tslp*

expression of sorted keratinocytes (KCs) (B) and proportion of total ILCs, IL-5⁺ ILC2s, and IL-17A⁺ ILC3s (C) from postnatal day 56 (P56) GF mouse skin with early or late mono-association with *S. lentus*. (D-G) Ear swelling (D) and H&E staining of ear skin (E) from each group of mice (scale bars = 100 μ m). Epidermis thickness (left) and accumulated leukocyte number (right) (F). *Tslp* expression in ear skin (G). (H) Experimental scheme for topical IAId treatment and mono-association with *S. lentus* and subsequent MC903-induced model. (I-L) Ear swelling (I) and H&E staining of ear skin (J) from each group of mice (scale bars = 100 μ m). Epidermis thickness (left) and accumulated leukocyte number (right) (K). *Tslp* expression in ear skin (L). (M) Experimental scheme for mono-association of wild-type (WT) *Staphylococcus aureus* (*S. aureus* WT) or *S. aureus* Δ ArAT mutant and subsequent MC903-induced model. (N-Q) Ear swelling (N) and H&E staining of ear skin (O) from each group of mice (scale bars = 50 μ m). Epidermis thickness (left) and accumulated leukocyte number (right) (P). *Tslp* expression in ear skin (Q). The GF control sample in (C) is identical to the GF control sample in Figure 12D because the experiment was performed simultaneously with the same control group. (B and C) Data are pooled from two independent experiments. (D-Q) Data are from one experiment representative of at least three independent experiments and displayed as mean \pm SEM; $n = 4-15$ mice per group. * $P < 0.05$, ** $P < 0.01$, and **** $P < 0.0001$, and ns, not significant.

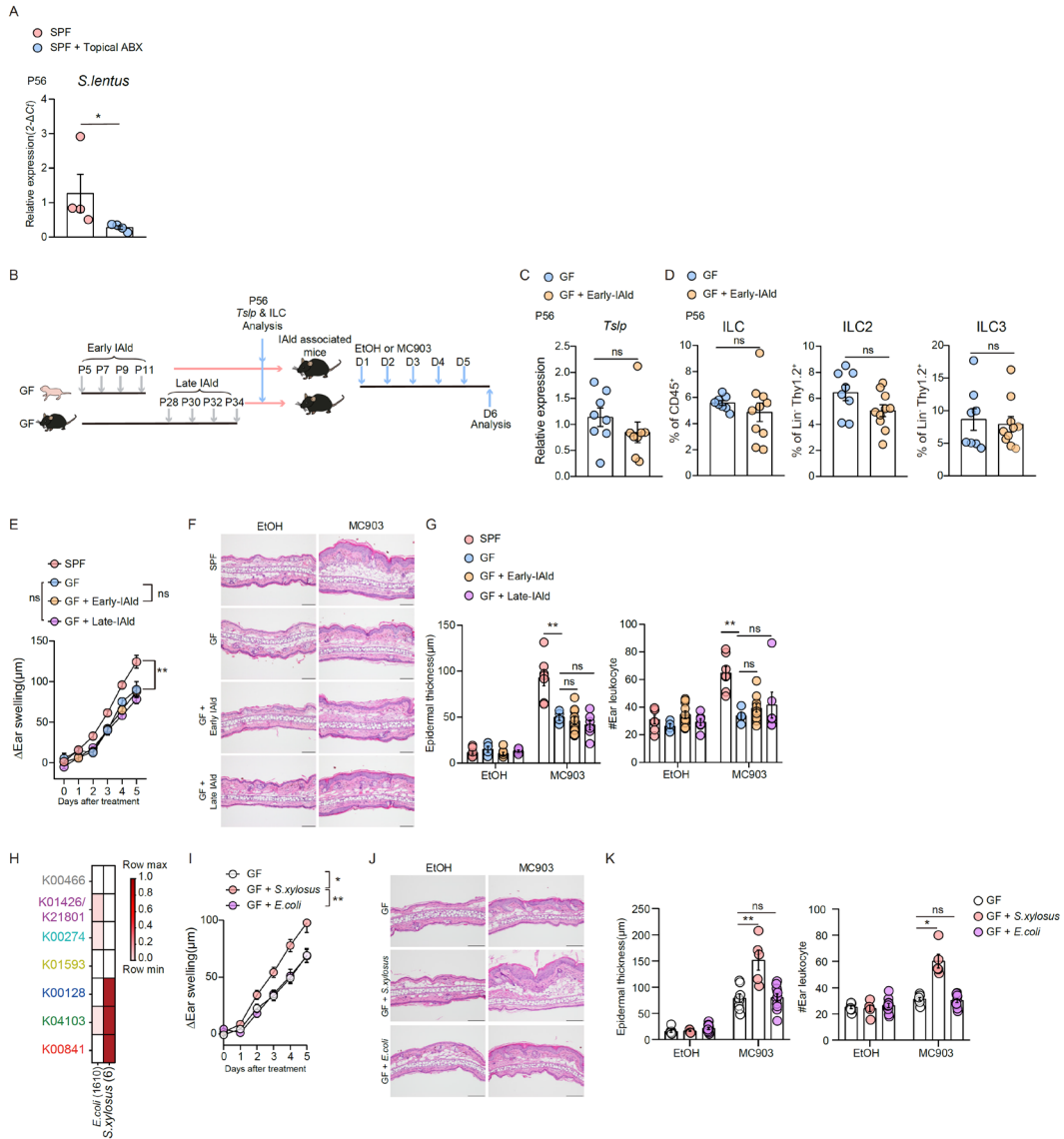


Figure 12. Bacterial unicity for IAId-producing potential leading to predisposition to AD-like inflammation. (A) Relative expression of *Staphylococcus lentus* (*S. lentus*) from skin swab samples of SPF mice with or without topical antibiotics (ABX) treatment. (B) Experimental protocol for topical IAId treatment for indicated time points and subsequent

MC903-induced atopic dermatitis (AD)-like inflammation model in postnatal day 56 (P56) GF mice. (C and D) *Tslp* expression of sorted keratinocytes (C) and proportion of total innate lymphoid cells (ILCs; CD45⁺Lin⁻Thy1.2⁺), IL-5⁺ ILC2s, and IL-17A⁺ ILC3s (D) from P56 GF mouse skin with early or late topical IAld treatment. (E) Ear swelling response of SPF, GF, GF + Early IAld, and GF + Late IAld mouse group treated with daily MC903. (F) H&E staining of ear skin from each group of mice (scale bars = 100 μ m). (G) Epidermal thickness (left) and accumulated leukocyte number (right) from each group of mice. (H) Presence of indole acetic acid pathway-related genes in *E. coli* and *S. xylosum*. (I) Ear swelling response of MC903 treatment in GF mice with mono-association of *S. xylosum* or *E. coli*. (J) H&E staining of ear skin from each group of mice (scale bars = 100 μ m). (K) Epidermal thickness (left) and accumulated leukocyte number (right) from each group of mice. (D) The GF control sample is identical to the GF control sample in Figure 11C because the experiment was performed simultaneously with the same control group. (n=8-10 per group, pooled from two independent experiments.) Data are from one experiment representative of at least two independent experiments and displayed as mean \pm SEM; *n* = 4-10 mice per group. ABX, antibiotics; GF, germ free; IAld, indole-3-aldehyde; ILCs, innate lymphoid cells; ns, not significant; P, postnatal day; SPF, Specific pathogen free. **P* < 0.05 and ***P* < 0.01.

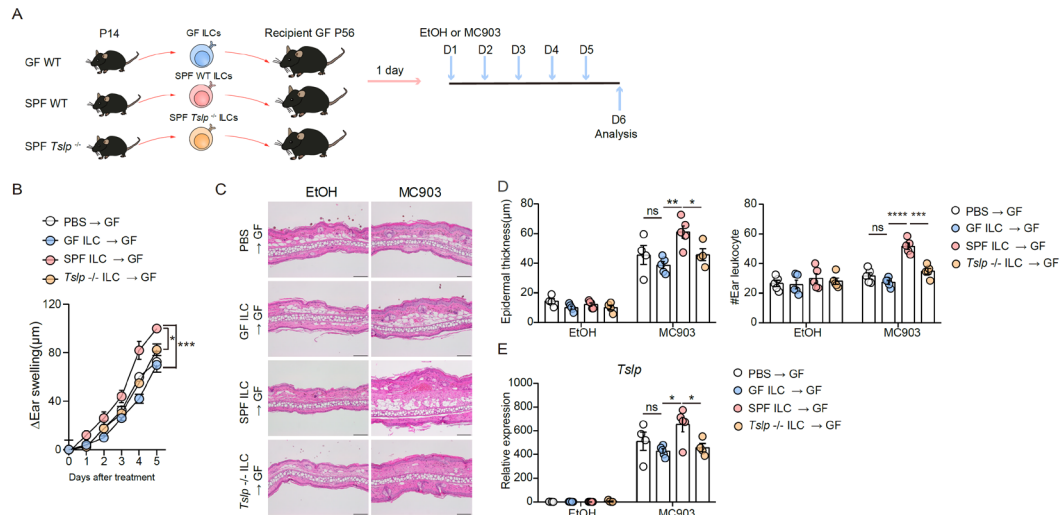


Figure 13. Neonatal skin microbe-TSLP-ILC2 priming axis contributes to AD-like inflammation in adulthood. (A) Experimental scheme for adoptive transfer of neonatal ILCs sorted from the indicated mice to recipient GF adult mice by intradermal injection and subsequent MC903-induced model. (B and C) Ear swelling (B) and H&E staining of ear skin (C) from each group of mice (scale bars = 100 μm). (D) Epidermis thickness (left) and accumulated leukocyte number (right). (E) *Tslp* expression of ear skin. Data are from one experiment representative of at least three independent experiments and displayed as mean ± SEM; $n = 4-5$ mice per group. $*P < 0.05$, $**P < 0.01$, $***P < 0.001$, and $****P < 0.0001$, and ns, not significant.

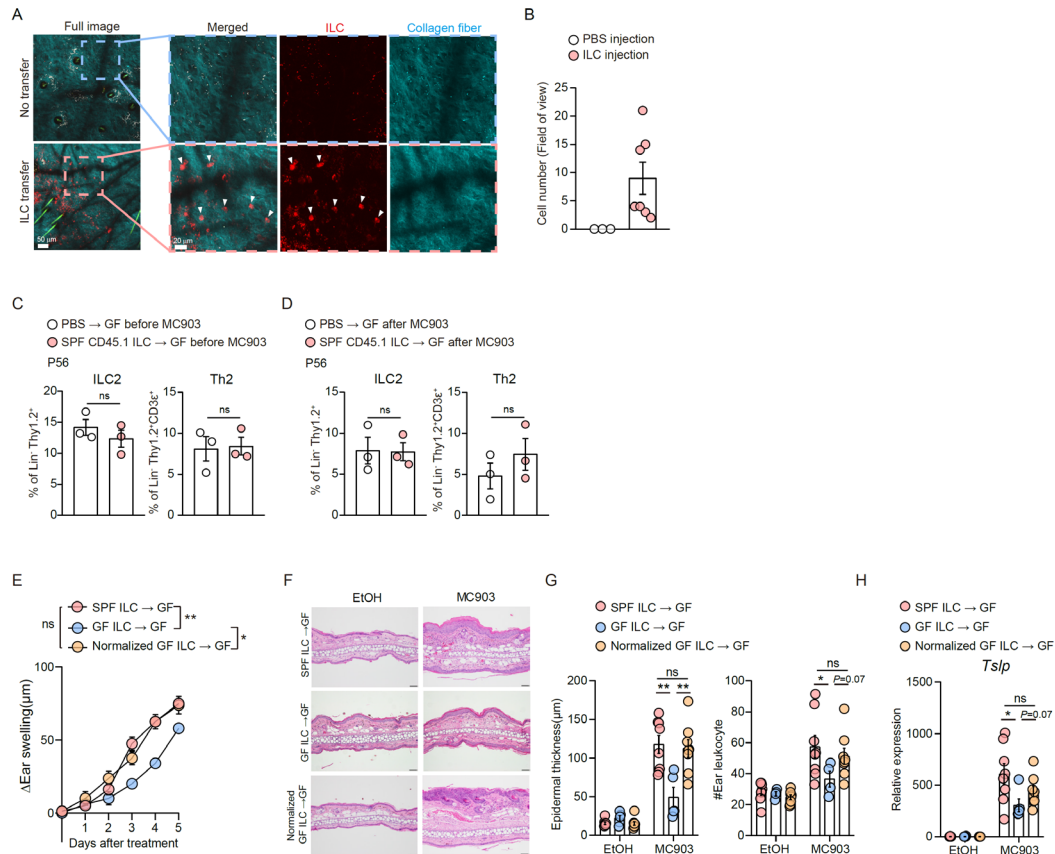


Figure 14. Different extent of postnatal ILC2 priming between SPF and GF skin leads to different severity of AD-like inflammation. (A) Two-photon microscopy images of transferred innate lymphoid cells (ILCs; $CD45^+Lin^-Thy1.2^+$; shown in red) in the ear skin of recipient GF mice. Arrowheads (white) indicate transferred ILCs. (B) Summarized graph for number of transferred ILCs per field of view. (C and D) Frequency of host ILC2s ($CD45.2^+Lin^-Thy1.2^+IL-5^+$) and Th2 cells ($CD45.2^+Lin^-Thy1.2^+CD3\epsilon^+IL-4^+IL-5^+IL-13^+$; Lin excepting $CD3\epsilon$) in recipient GF mice transferred with donor ILCs before (C) and after (D) MC903 treatment. (E) Ear swelling response of GF mice transferred with indicated ILCs 1 day prior to daily MC903 treatment. (F) H&E staining of ear skin from each group of mice (scale bars = 50 μ m). (G) Epidermal thickness (left) and accumulated leukocyte

number (right) from each group of mice. (H) *Tsfp* expression of ear skin from each group of mice. (A-D) Data are from one experiment representative of at least two independent experiments and displayed as mean \pm SEM; $n = 3-5$ mice per group. (E-H) Data are from one experiment representative of at least two independent experiments and displayed as mean \pm SEM; $n = 4-8$ mice per group. GF, germ free; ILCs, innate lymphoid cells; ns, not significant; P, postnatal day; SPF, Specific pathogen free; Th2 cells, T helper 2 cells. $*P < 0.05$, and $**P < 0.01$.

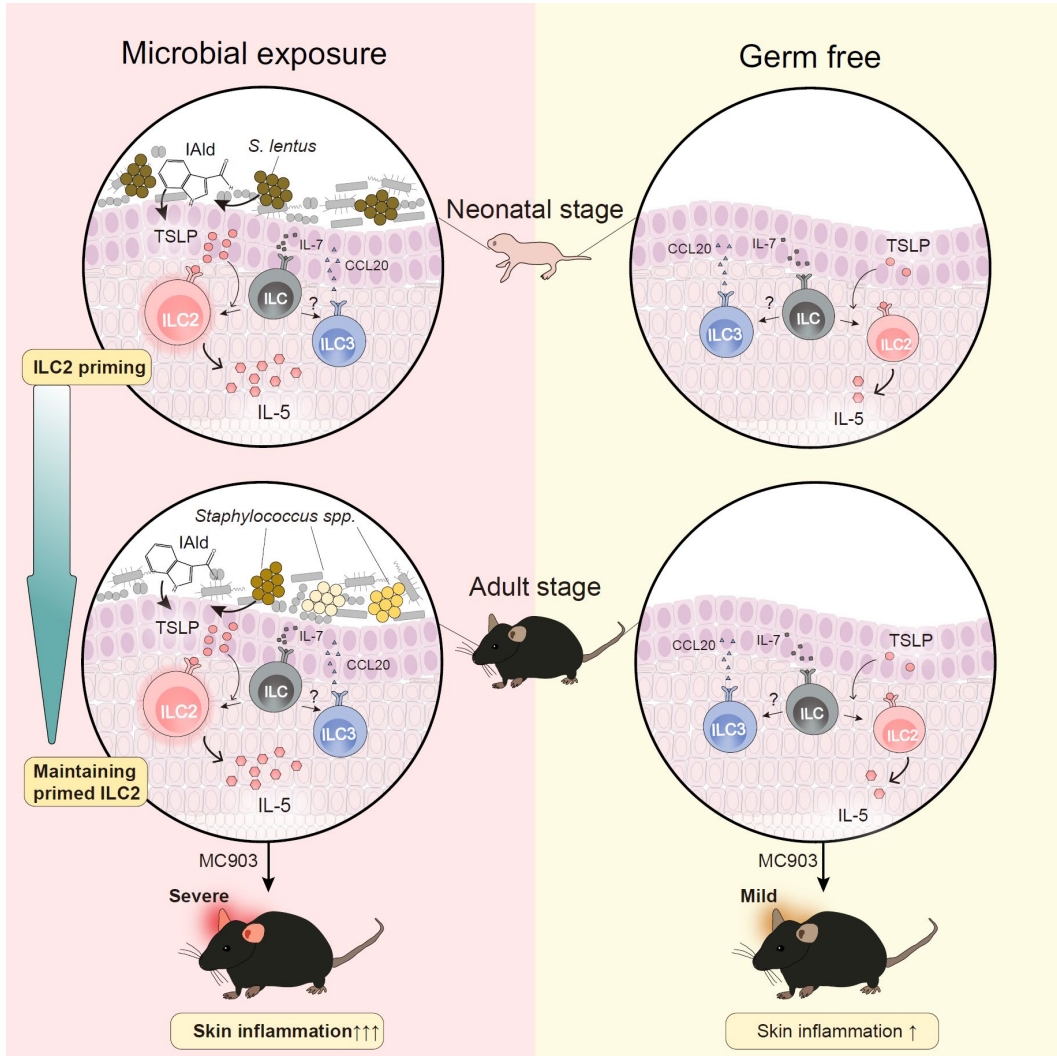


Figure 15. Skin microbe-dependent TSLP-ILC2 Priming Axis in early life is co-opted in allergic inflammation.

Table 1. Primers used in this study

PRIMER NAME	SEQUENCE
ArAT 900 For	5'-ACCGGCATTGTTAGAGGATTTGAATGG-3'
ArAT 780 Rev	5'-GGAGAGGAATATAACTCGGTAG-3'
ArAT(N177) Erm For	5'-GCTGTCTTGTTAAATTATCCGACTACCTTAGA AGCAAACCTAAGAGTG-3'
ArAT(N177) Erm Rev	5'-CACTCTTAAGTTTGCTTCTAAGGTAGTCGGA TAATTTAACAAGACAGC-3'
Erm ArAT(N177) For	5'-CTAAAGGGAATGGAGACCGGGATCCAACCTG GCGTAGTTTTAAAAAGAAA-3'
Erm ArAT(N177) Rev	5'-TTTCTTTTTTAAACTACGCCAGTTGGATCCC GGTCTCCATTCCTTTAG-3'
ArAT mut 100 For	5'-ATCGCAATGACTGCGTTTCT-3'
ArAT mut 486 Rev	5'-TGCTGCTGGAGAACTCACAA-3'
<i>mHprt</i> For	5'-TCAGTCAACGGGGGACATAAA-3'
<i>mHprt</i> Rev	5'-GGGGCTGTACTGCTTAACCAG-3'
<i>mTslp</i> For	5'-TCGAGGACTGTGAGAGCAAGCCAG-3'
<i>mTslp</i> Rev	5'-CTGGAGATTGCATGAAGGAATACCA-3'
<i>mI133</i> For	5'-ACCAGGTGCTACTACGCTAC-3
<i>mI133</i> Rev	5'-TCACCATCAGCTTCTTCCCA-3'
<i>mI17</i> For	5'-TGCAGTCCCAGTCATCATGA-3'
<i>mI17</i> Rev	5'-GGCAGCAGAACAAGGATCAG-3'
<i>mCcl20</i> For	5'-TTGCTTTGGCATGGGTAAGT-3'
<i>mCcl20</i> Rev	5'-TCGTAGTTGCTTGCTGCTTCTG-3'
<i>mI118</i> For	5'- ACTTTGGCCGACTTCACTGT -3'
<i>mI118</i> Rev	5'- GGGTTCACTGGCACTTTGAT-3'
<i>hTSLP</i> For	5'-GGCCACATTGCCTTACTGAA-3'
<i>hTSLP</i> Rev	5'-TGGGCACCAGATAGCTAAGG-3'
<i>hGAPDH</i> For	5'-CTGGGCTACACTGAGCACC-3'
<i>hGAPDH</i> Rev	5'-AAGTGGTCGTTGAGGGCAATG-3'
<i>S.lentus</i> 239 For:	5'-TGACTGATGAAGCACGCACA-3'
<i>S.lentus</i> 531 Rev:	5'-TCTTGCTTCTTCTTCGCTCCA-3'
16S 27 For	5'- AGAGTTTGATCCTGGCTCAG-3'
16S 534 Rev	5'- ATTACCGCGGCTGCTGG-3'

IV. DISCUSSION

Although previous studies have revealed the role of skin commensal microbes in shaping the quality of immunological and physiological responses following exposure in adulthood,^{4, 11, 84, 85} it remains largely unclear whether postnatal exposure to microbiota induces the long-lasting immune imprinting and consequently influences the extent of skin inflammation later in life. Here, we uncover a previously unappreciated role of early colonization of IA1d-producing skin commensal *Staphylococcus* species in the regulation of TSLP-dependent postnatal ILC2 priming, which contributes to AD-like inflammation in adults.

ILCs arise from both prenatal and postnatal progenitors that seed peripheral tissues and actively differentiate into specific ILC subsets.⁸⁶⁻⁸⁸ ILC2s are largely tissue-resident cells that promote local type 2 immune responses through *in situ* expansion and release of type 2 cytokines upon stimulation with a set of epithelial-driven factors, including IL-25, IL-33, and TSLP.^{61, 89-92} Recent works have shown that ILC2s undergo postnatal maturation and priming to produce maximal amounts of effector cytokines,^{65, 89, 93} and the gene expression program of intestinal ILC2 signature is significantly reduced in the absence of microbiota,⁶⁸ suggesting a potential role for commensal microbes in regulating ILC2 priming. In line with previous studies, we found that ILC2 development in the skin is highly dynamic during the first 2 weeks of life and that postnatal priming of ILC2s occurs following early exposure to commensal microbiota. Notably, microbe-dependent expression of TSLP in postnatal KCs critically induces ILC2 priming. Since ILC2s in different tissues exhibit distinct responsiveness to activating cytokines, such as TSLP in the skin and IL-33 in the lung,^{65, 86, 92} we speculate that tissue-specific imprinting signals for postnatal ILC2s priming may preemptively establish different ILC2 responses in each tissue. Previous studies have shown that IL-5 expression in skin ILC2s is comparable between SPF and GF conditions in neonatal and adult mice.^{69, 89} Discrepancies compared to the results reported herein may reflect the different methods used to measure IL-5 expression. We evaluated fully competent ILC2s capable of producing IL-5 protein after stimulation with PMA and

ionomycin by flow cytometry, while other studies analyzed IL-5 transcript levels in ILC2s by reporter mice or quantitative PCR. Therefore, further integrative approaches to measure both transcript and protein levels of representative lineage markers will provide more reliable interpretation of ILC2 biology. In addition, unlike ILC2s, regulatory mechanisms of ILC3 expansion and activation in neonatal stages remain largely unexplored in the skin. Our results demonstrate a critical involvement of the CCL20/CCR6 chemokine system in the postnatal priming of skin ILC3s as seen in gut ILC3s.⁷⁷ However, the dispensable role of skin commensals in postnatal *Ccl20* expression and ILC3 priming implies unrecognized intrinsic cues in establishing ILC3 activity early in life, thus warranting further study.

Commensal bacteria-derived metabolites actively modulate local immune homeostasis by licensing the functional properties of immune cells.^{16, 22, 31, 94-96} Our data revealed that colonization with *S. lentus*, the dominant *Staphylococcus* species in early postnatal skin, sufficiently induces ILC2 priming by promoting *Tslp* expression in KCs. Based on comparative whole-genome sequencing analysis involving *S. lentus* isolates in our study, pathway-related genes for IAld-generating Trp-indole metabolism were highly conserved across *Staphylococcus* species and were functionally relevant to TSLP-dependent ILC2 priming *in vivo*. Previous studies reported that IAld levels are reduced in human AD lesional skin and that topical application of IAld inhibits TSLP expression in adult KCs under MC903-induced inflammation in an aryl hydrocarbon receptor (AhR)-dependent manner.³⁵ However, compared to the relatively well-known anti-inflammatory effects of Trp metabolites, their fundamental role in steady-state skin, especially in the regulation of postnatal imprinting of the skin immune system, is poorly understood yet. In the current study, we found that skin commensal *Staphylococcus*-derived IAld contributes to a previously unrecognized ILC2 priming axis by inducing TSLP from KCs. Currently, how IAld differentially regulates TSLP expression between inflammatory and steady-state skin conditions remains largely unknown. Previous reports have shown that activation of AhR negatively regulates TSLP expression in KCs upon inflammatory stimuli by inhibiting acetylation-dependent DNA-binding of NF- κ B to the *TSLP* promoter.⁹⁷ As the *TSLP*

promoter contains multiple AhR-binding elements,³⁵ it would be worthwhile to explore whether IALD-mediated AhR activation directly or indirectly regulates homeostatic expression of TSLP in KCs and subsequent ILC2 priming.

Host-microbe interactions during specific time window of early life can result in persistent immune imprinting, thereby affecting the quality of immune responses in adulthood.^{63, 98, 99} Our results demonstrate that early postnatal exposure to commensal microbiota, but not later exposure, induces ILC2 priming that predisposes the host to AD-like inflammation. It has been recognized that different types of immune cells have distinct window periods for functional priming.^{17, 63, 100} Previous studies, together with the dynamic development of skin ILC2s reported herein, suggest that priming of ILC2s occurs as early as 2 weeks of postnatal life, providing a unique window period to potentially modify their activity.^{65, 89} However, our data also demonstrate that susceptibility to AD-like inflammation in adulthood requires constitutive colonization with commensal *Staphylococci* after initial ILC2 priming. Therefore, further investigation is needed to determine whether commensal bacteria directly regulate the cellular identity or homeostatic maintenance of early primed ILC2s through sustained induction of local TSLP, as shown by reduced ILC2s in *Tslp*-deficient mouse skin.⁶¹

In conclusion, early exposure to commensal microbes establishes an important arsenal for type 2 innate immunity in the skin through mutual crosstalk with the developing epithelial barrier. Co-optation of the skin microbiota-dependent ILC2 priming axis in allergic inflammation suggests the possibility for proactive regulation of early symbiotic microbes to modify the extent of type 2 immunity later in life. Therefore, it would be noteworthy to investigate whether postnatal dysbiosis driven by genetic predisposition to AD alters the magnitude of ILC2 priming and subsequently contributes to the future development of AD in humans.^{24, 25, 101} Further mechanistic exploration of the skin microbiota-ILC2 priming axis will lead to the development of potential disease-modifying strategies to enable early intervention in allergic skin diseases.

V. CONCLUSION

We demonstrated that early postnatal colonization with IAld-producing *Staphylococcus* species induces TSLP-mediated early ILC2 priming. In addition, ILC2 priming early in life is co-opted in allergic skin inflammation in adulthood.

REFERENCES

1. Sommer F, Backhed F. The gut microbiota--masters of host development and physiology. *Nat Rev Microbiol.* 2013 Apr;11(4):227-38.
2. Grice EA, Segre JA. The skin microbiome. *Nat Rev Microbiol.* 2011 Apr;9(4):244-53.
3. Pasparakis M, Haase I, Nestle FO. Mechanisms regulating skin immunity and inflammation. *Nat Rev Immunol.* 2014 May;14(5):289-301.
4. Kobayashi T, Naik S, Nagao K. Choreographing Immunity in the Skin Epithelial Barrier. *Immunity.* 2019 Mar 19;50(3):552-65.
5. Chen YE, Fischbach MA, Belkaid Y. Skin microbiota-host interactions. *Nature.* 2018 Jan 24;553(7689):427-36.
6. Byrd AL, Belkaid Y, Segre JA. The human skin microbiome. *Nat Rev Microbiol.* 2018 Mar;16(3):143-55.
7. Meisel JS, Sfyroera G, Bartow-McKenney C, Gimblet C, Bugayev J, Horwinski J, et al. Commensal microbiota modulate gene expression in the skin. *Microbiome.* 2018 Jan 30;6(1):20.
8. Uberoi A, Bartow-McKenney C, Zheng Q, Flowers L, Campbell A, Knight SAB, et al. Commensal microbiota regulates skin barrier function and repair via signaling through the aryl hydrocarbon receptor. *Cell Host Microbe.* 2021 Aug 11;29(8):1235-48 e8.
9. Wang G, Sweren E, Liu H, Wier E, Alphonse MP, Chen R, et al. Bacteria induce skin regeneration via IL-1beta signaling. *Cell Host Microbe.* 2021 May 12;29(5):777-91 e6.
10. Wang G, Sweren E, Andrews W, Li Y, Chen J, Xue Y, et al. Commensal microbiome promotes hair follicle regeneration by inducing keratinocyte HIF-1alpha signaling and glutamine metabolism. *Sci Adv.* 2023 Jan 4;9(1):eabo7555.
11. Belkaid Y, Harrison OJ. Homeostatic Immunity and the Microbiota. *Immunity.* 2017 Apr 18;46(4):562-76.
12. Patra V, Wagner K, Arulampalam V, Wolf P. Skin Microbiome Modulates the

- Effect of Ultraviolet Radiation on Cellular Response and Immune Function. *iScience*. 2019 May 31;15:211-22.
13. Naik S, Bouladoux N, Wilhelm C, Molloy MJ, Salcedo R, Kastenmuller W, et al. Compartmentalized control of skin immunity by resident commensals. *Science*. 2012 Aug 31;337(6098):1115-9.
 14. Naik S, Bouladoux N, Linehan JL, Han SJ, Harrison OJ, Wilhelm C, et al. Commensal-dendritic-cell interaction specifies a unique protective skin immune signature. *Nature*. 2015 Apr 2;520(7545):104-8.
 15. Linehan JL, Harrison OJ, Han SJ, Byrd AL, Vujkovic-Cvijin I, Villarino AV, et al. Non-classical Immunity Controls Microbiota Impact on Skin Immunity and Tissue Repair. *Cell*. 2018 Feb 8;172(4):784-96 e18.
 16. Harrison OJ, Linehan JL, Shih HY, Bouladoux N, Han SJ, Smelkinson M, et al. Commensal-specific T cell plasticity promotes rapid tissue adaptation to injury. *Science*. 2019 Jan 4;363(6422).
 17. Dhariwala MO, Scharschmidt TC. Baby's skin bacteria: first impressions are long-lasting. *Trends Immunol*. 2021 Dec;42(12):1088-99.
 18. Dwyer LR, Scharschmidt TC. Early life host-microbe interactions in skin. *Cell Host Microbe*. 2022 May 11;30(5):684-95.
 19. Scharschmidt TC, Vasquez KS, Truong HA, Gearty SV, Pauli ML, Nosbaum A, et al. A Wave of Regulatory T Cells into Neonatal Skin Mediates Tolerance to Commensal Microbes. *Immunity*. 2015 Nov 17;43(5):1011-21.
 20. Scharschmidt TC, Vasquez KS, Pauli ML, Leitner EG, Chu K, Truong HA, et al. Commensal Microbes and Hair Follicle Morphogenesis Coordinately Drive Treg Migration into Neonatal Skin. *Cell Host Microbe*. 2017 Apr 12;21(4):467-77 e5.
 21. Leech JM, Dhariwala MO, Lowe MM, Chu K, Merana GR, Cornuot C, et al. Toxin-Triggered Interleukin-1 Receptor Signaling Enables Early-Life Discrimination of Pathogenic versus Commensal Skin Bacteria. *Cell Host Microbe*. 2019 Dec 11;26(6):795-809 e5.

22. Constantinides MG, Link VM, Tamoutounour S, Wong AC, Perez-Chaparro PJ, Han SJ, et al. MAIT cells are imprinted by the microbiota in early life and promote tissue repair. *Science*. 2019 Oct 25;366(6464).
23. Capone KA, Dowd SE, Stamatias GN, Nikolovski J. Diversity of the human skin microbiome early in life. *J Invest Dermatol*. 2011 Oct;131(10):2026-32.
24. Meylan P, Lang C, Mermoud S, Johannsen A, Norrenberg S, Hohl D, et al. Skin Colonization by *Staphylococcus aureus* Precedes the Clinical Diagnosis of Atopic Dermatitis in Infancy. *J Invest Dermatol*. 2017 Dec;137(12):2497-504.
25. Nakamura Y, Takahashi H, Takaya A, Inoue Y, Katayama Y, Kusuya Y, et al. *Staphylococcus Agr* virulence is critical for epidermal colonization and associates with atopic dermatitis development. *Sci Transl Med*. 2020 Jul 8;12(551).
26. Postler TS, Ghosh S. Understanding the Holobiont: How Microbial Metabolites Affect Human Health and Shape the Immune System. *Cell Metab*. 2017 Jul 5;26(1):110-30.
27. Rooks MG, Garrett WS. Gut microbiota, metabolites and host immunity. *Nat Rev Immunol*. 2016 May 27;16(6):341-52.
28. Roager HM, Licht TR. Microbial tryptophan catabolites in health and disease. *Nat Commun*. 2018 Aug 17;9(1):3294.
29. Henrick BM, Rodriguez L, Lakshmikanth T, Pou C, Henckel E, Arzoomand A, et al. Bifidobacteria-mediated immune system imprinting early in life. *Cell*. 2021 Jul 22;184(15):3884-98 e11.
30. Spivak I, Fluhr L, Elinav E. Local and systemic effects of microbiome-derived metabolites. *EMBO Rep*. 2022 Oct 6;23(10):e55664.
31. Zelante T, Iannitti RG, Cunha C, De Luca A, Giovannini G, Pieraccini G, et al. Tryptophan catabolites from microbiota engage aryl hydrocarbon receptor and balance mucosal reactivity via interleukin-22. *Immunity*. 2013 Aug 22;39(2):372-85.
32. Venkatesh M, Mukherjee S, Wang H, Li H, Sun K, Benechet AP, et al. Symbiotic bacterial metabolites regulate gastrointestinal barrier function via the xenobiotic

- sensor PXR and Toll-like receptor 4. *Immunity*. 2014 Aug 21;41(2):296-310.
33. Li Y, Liu N, Ge Y, Yang Y, Ren F, Wu Z. Tryptophan and the innate intestinal immunity: Crosstalk between metabolites, host innate immune cells, and microbiota. *Eur J Immunol*. 2022 Jun;52(6):856-68.
 34. Chng KR, Tay AS, Li C, Ng AH, Wang J, Suri BK, et al. Whole metagenome profiling reveals skin microbiome-dependent susceptibility to atopic dermatitis flare. *Nat Microbiol*. 2016 Jul 11;1(9):16106.
 35. Yu J, Luo Y, Zhu Z, Zhou Y, Sun L, Gao J, et al. A tryptophan metabolite of the skin microbiota attenuates inflammation in patients with atopic dermatitis through the aryl hydrocarbon receptor. *J Allergy Clin Immunol*. 2019 Jun;143(6):2108-19 e12.
 36. Kang YK, Park JS, Lee CS, Yeom YI, Chung AS, Lee KK. Efficient integration of short interspersed element-flanked foreign DNA via homologous recombination. *J Biol Chem*. 1999 Dec 17;274(51):36585-91.
 37. Jeon J, Park JS, Min B, Chung SK, Kim MK, Kang YK. Retroelement Insertion in a CRISPR/Cas9 Editing Site in the Early Embryo Intensifies Genetic Mosaicism. *Front Cell Dev Biol*. 2019;7:273.
 38. Tauer C, Heintz S, Egger E, Heiss S, Grabherr R. Tuning constitutive recombinant gene expression in *Lactobacillus plantarum*. *Microb Cell Fact*. 2014 Nov 20;13:150.
 39. Bae T, Schneewind O. Allelic replacement in *Staphylococcus aureus* with inducible counter-selection. *Plasmid*. 2006 Jan;55(1):58-63.
 40. Kim BS, Siracusa MC, Saenz SA, Noti M, Monticelli LA, Sonnenberg GF, et al. TSLP elicits IL-33-independent innate lymphoid cell responses to promote skin inflammation. *Sci Transl Med*. 2013 Jan 30;5(170):170ra16.
 41. Grice EA, Kong HH, Conlan S, Deming CB, Davis J, Young AC, et al. Topographical and temporal diversity of the human skin microbiome. *Science*. 2009 May 29;324(5931):1190-2.
 42. Kim D, Langmead B, Salzberg SL. HISAT: a fast spliced aligner with low memory requirements. *Nat Methods*. 2015 Apr;12(4):357-60.

43. Pertea M, Pertea GM, Antonescu CM, Chang TC, Mendell JT, Salzberg SL. StringTie enables improved reconstruction of a transcriptome from RNA-seq reads. *Nat Biotechnol.* 2015 Mar;33(3):290-5.
44. Pertea M, Kim D, Pertea GM, Leek JT, Salzberg SL. Transcript-level expression analysis of RNA-seq experiments with HISAT, StringTie and Ballgown. *Nat Protoc.* 2016 Sep;11(9):1650-67.
45. Wood DE, Lu J, Langmead B. Improved metagenomic analysis with Kraken 2. *Genome Biol.* 2019 Nov 28;20(1):257.
46. Lu JB, F.P., Thielen, P., Salzberg, S.L. Bracken: estimating species abundance in metagenomics data. *PeerJ Computer Science.* 2017;3.
47. Li D, Luo R, Liu CM, Leung CM, Ting HF, Sadakane K, et al. MEGAHIT v1.0: A fast and scalable metagenome assembler driven by advanced methodologies and community practices. *Methods.* 2016 Jun 1;102:3-11.
48. Rho M, Tang H, Ye Y. FragGeneScan: predicting genes in short and error-prone reads. *Nucleic Acids Res.* 2010 Nov;38(20):e191.
49. Buchfink B, Xie C, Huson DH. Fast and sensitive protein alignment using DIAMOND. *Nat Methods.* 2015 Jan;12(1):59-60.
50. Kanehisa M, Goto S. KEGG: kyoto encyclopedia of genes and genomes. *Nucleic Acids Res.* 2000 Jan 1;28(1):27-30.
51. Fu L, Niu B, Zhu Z, Wu S, Li W. CD-HIT: accelerated for clustering the next-generation sequencing data. *Bioinformatics.* 2012 Dec 1;28(23):3150-2.
52. Rubio-Largo A, Vanneschi L, Castelli M, Vega-Rodriguez MA. A Characteristic-Based Framework for Multiple Sequence Aligners. *IEEE Trans Cybern.* 2018 Jan;48(1):41-51.
53. Tamura K, Stecher G, Kumar S. MEGA11: Molecular Evolutionary Genetics Analysis Version 11. *Mol Biol Evol.* 2021 Jun 25;38(7):3022-7.
54. Li M, Hener P, Zhang Z, Kato S, Metzger D, Chambon P. Topical vitamin D3 and low-calcemic analogs induce thymic stromal lymphopoietin in mouse keratinocytes

- and trigger an atopic dermatitis. *Proc Natl Acad Sci U S A*. 2006 Aug 1;103(31):11736-41.
55. Oetjen LK, Mack MR, Feng J, Whelan TM, Niu H, Guo CJ, et al. Sensory Neurons Co-opt Classical Immune Signaling Pathways to Mediate Chronic Itch. *Cell*. 2017 Sep 21;171(1):217-28 e13.
56. Naidoo K, Jagot F, van den Elsen L, Pellefigues C, Jones A, Luo H, et al. Eosinophils Determine Dermal Thickening and Water Loss in an MC903 Model of Atopic Dermatitis. *J Invest Dermatol*. 2018 Dec;138(12):2606-16.
57. Salimi M, Barlow JL, Saunders SP, Xue L, Gutowska-Owsiak D, Wang X, et al. A role for IL-25 and IL-33-driven type-2 innate lymphoid cells in atopic dermatitis. *J Exp Med*. 2013 Dec 16;210(13):2939-50.
58. Li C, Maillet I, Mackowiak C, Viala C, Di Padova F, Li M, et al. Experimental atopic dermatitis depends on IL-33R signaling via MyD88 in dendritic cells. *Cell Death Dis*. 2017 Apr 6;8(4):e2735.
59. Leyva-Castillo JM, Hener P, Jiang H, Li M. TSLP produced by keratinocytes promotes allergen sensitization through skin and thereby triggers atopic march in mice. *J Invest Dermatol*. 2013 Jan;133(1):154-63.
60. Walsh CM, Hill RZ, Schwendinger-Schreck J, Deguine J, Brock EC, Kucirek N, et al. Neutrophils promote CXCR3-dependent itch in the development of atopic dermatitis. *Elife*. 2019 Oct 21;8.
61. Kobayashi T, Voisin B, Kim DY, Kennedy EA, Jo JH, Shih HY, et al. Homeostatic Control of Sebaceous Glands by Innate Lymphoid Cells Regulates Commensal Bacteria Equilibrium. *Cell*. 2019 Feb 21;176(5):982-97 e16.
62. Alkon N, Bauer WM, Krausgruber T, Goh I, Griss J, Nguyen V, et al. Single-cell analysis reveals innate lymphoid cell lineage infidelity in atopic dermatitis. *J Allergy Clin Immunol*. 2022 Feb;149(2):624-39.
63. Hornef MW, Torow N. 'Layered immunity' and the 'neonatal window of opportunity' - timed succession of non-redundant phases to establish mucosal host-

- microbial homeostasis after birth. *Immunology*. 2020 Jan;159(1):15-25.
64. Gensollen T, Iyer SS, Kasper DL, Blumberg RS. How colonization by microbiota in early life shapes the immune system. *Science*. 2016 Apr 29;352(6285):539-44.
 65. Steer CA, Matha L, Shim H, Takei F. Lung group 2 innate lymphoid cells are trained by endogenous IL-33 in the neonatal period. *JCI Insight*. 2020 Jul 23;5(14).
 66. Zhao M, Shao F, Yu D, Zhang J, Liu Z, Ma J, et al. Maturation and specialization of group 2 innate lymphoid cells through the lung-gut axis. *Nat Commun*. 2022 Dec 9;13(1):7600.
 67. Bando JK, Liang HE, Locksley RM. Identification and distribution of developing innate lymphoid cells in the fetal mouse intestine. *Nat Immunol*. 2015 Feb;16(2):153-60.
 68. Gury-BenAri M, Thaïss CA, Serafini N, Winter DR, Giladi A, Lara-Astiaso D, et al. The Spectrum and Regulatory Landscape of Intestinal Innate Lymphoid Cells Are Shaped by the Microbiome. *Cell*. 2016 Aug 25;166(5):1231-46 e13.
 69. Ricardo-Gonzalez RR, Van Dyken SJ, Schneider C, Lee J, Nussbaum JC, Liang HE, et al. Tissue signals imprint ILC2 identity with anticipatory function. *Nat Immunol*. 2018 Oct;19(10):1093-9.
 70. Halim TY, Krauss RH, Sun AC, Takei F. Lung natural helper cells are a critical source of Th2 cell-type cytokines in protease allergen-induced airway inflammation. *Immunity*. 2012 Mar 23;36(3):451-63.
 71. Mirchandani AS, Besnard AG, Yip E, Scott C, Bain CC, Cerovic V, et al. Type 2 innate lymphoid cells drive CD4⁺ Th2 cell responses. *J Immunol*. 2014 Mar 1;192(5):2442-8.
 72. Gurram RK, Zhu J. Orchestration between ILC2s and Th2 cells in shaping type 2 immune responses. *Cell Mol Immunol*. 2019 Mar;16(3):225-35.
 73. Gurram RK, Wei D, Yu Q, Butcher MJ, Chen X, Cui K, et al. Crosstalk between ILC2s and Th2 cells varies among mouse models. *Cell Rep*. 2023 Feb 2;42(2):112073.
 74. Lange-Asschenfeldt B, Marenbach D, Lang C, Patzelt A, Ulrich M, Maltusch A,

- et al. Distribution of bacteria in the epidermal layers and hair follicles of the human skin. *Skin Pharmacol Physiol*. 2011;24(6):305-11.
75. Markovic I, Savvides SN. Modulation of Signaling Mediated by TSLP and IL-7 in Inflammation, Autoimmune Diseases, and Cancer. *Front Immunol*. 2020;11:1557.
76. Ebina-Shibuya R, Leonard WJ. Role of thymic stromal lymphopoietin in allergy and beyond. *Nat Rev Immunol*. 2023 Jan;23(1):24-37.
77. Bouskra D, Brezillon C, Berard M, Werts C, Varona R, Boneca IG et al. Lymphoid tissue genesis induced by commensals through NOD1 regulates intestinal homeostasis. *Nature*. 2008 Nov 27;456(7221):507-10.
78. Al Nabhani Z, Dulauroy S, Marques R, Cousu C, Al Bounny S, Dejardin F, et al. A Weaning Reaction to Microbiota Is Required for Resistance to Immunopathologies in the Adult. *Immunity*. 2019 May 21;50(5):1276-88 e5.
79. Andersen MS, Hannezo E, Ulyanchenko S, Estrach S, Antoku Y, Pisano S, et al. Tracing the cellular dynamics of sebaceous gland development in normal and perturbed states. *Nat Cell Biol*. 2019 Aug;21(8):924-32.
80. Singh TP, Carvalho AM, Sacramento LA, Grice EA, Scott P. Microbiota instruct IL-17A-producing innate lymphoid cells to promote skin inflammation in cutaneous leishmaniasis. *PLoS Pathog*. 2021 Oct;17(10):e1009693.
81. Kim Y, Lee YS, Yang JY, Lee SH, Park YY, Kweon MN. The resident pathobiont *Staphylococcus xylosus* in *Nfkbiz*-deficient skin accelerates spontaneous skin inflammation. *Sci Rep*. 2017 Jul 24;7(1):6348.
82. Krautkramer KA, Fan J, Backhed F. Gut microbial metabolites as multi-kingdom intermediates. *Nat Rev Microbiol*. 2021 Feb;19(2):77-94.
83. Ye X, Li H, Anjum K, Zhong X, Miao S, Zheng G, et al. Dual Role of Indoles Derived From Intestinal Microbiota on Human Health. *Front Immunol*. 2022;13:903526.
84. Belkaid Y, Segre JA. Dialogue between skin microbiota and immunity. *Science*. 2014 Nov 21;346(6212):954-9.

85. Flowers L, Grice EA. The Skin Microbiota: Balancing Risk and Reward. *Cell Host Microbe*. 2020 Aug 12;28(2):190-200.
86. Meininger I, Carrasco A, Rao A, Soini T, Kokkinou E, Mjosberg J. Tissue-Specific Features of Innate Lymphoid Cells. *Trends Immunol*. 2020 Oct;41(10):902-17.
87. Cherrier DE, Serafini N, Di Santo JP. Innate Lymphoid Cell Development: A T Cell Perspective. *Immunity*. 2018 Jun 19;48(6):1091-103.
88. Ghaedi M, Takei F. Innate lymphoid cell development. *J Allergy Clin Immunol*. 2021 May;147(5):1549-60.
89. Schneider C, Lee J, Koga S, Ricardo-Gonzalez RR, Nussbaum JC, Smith LK, et al. Tissue-Resident Group 2 Innate Lymphoid Cells Differentiate by Layered Ontogeny and In Situ Perinatal Priming. *Immunity*. 2019 Jun 18;50(6):1425-38 e5.
90. Gasteiger G, Fan X, Dikiy S, Lee SY, Rudensky AY. Tissue residency of innate lymphoid cells in lymphoid and nonlymphoid organs. *Science*. 2015 Nov 20;350(6263):981-5.
91. Moro K, Kabata H, Tanabe M, Koga S, Takeno N, Mochizuki M, et al. Interferon and IL-27 antagonize the function of group 2 innate lymphoid cells and type 2 innate immune responses. *Nat Immunol*. 2016 Jan;17(1):76-86.
92. Kobayashi T, Moro K. Tissue-Specific Diversity of Group 2 Innate Lymphoid Cells in the Skin. *Front Immunol*. 2022;13:885642.
93. Steer CA, Martinez-Gonzalez I, Ghaedi M, Allinger P, Matha L, Takei F. Group 2 innate lymphoid cell activation in the neonatal lung drives type 2 immunity and allergen sensitization. *J Allergy Clin Immunol*. 2017 Aug;140(2):593-5 e3.
94. Agus A, Planchais J, Sokol H. Gut Microbiota Regulation of Tryptophan Metabolism in Health and Disease. *Cell Host Microbe*. 2018 Jun 13;23(6):716-24.
95. Song X, Sun X, Oh SF, Wu M, Zhang Y, Zheng W, et al. Microbial bile acid metabolites modulate gut RORgamma(+) regulatory T cell homeostasis. *Nature*. 2020 Jan;577(7790):410-5.
96. Li W, Hang S, Fang Y, Bae S, Zhang Y, Zhang M, et al. A bacterial bile acid

- metabolite modulates T(reg) activity through the nuclear hormone receptor NR4A1. *Cell Host Microbe*. 2021 Sep 8;29(9):1366-77 e9.
97. Jeong H, Shin JY, Kim MJ, Na J, Ju BG. Activation of Aryl Hydrocarbon Receptor Negatively Regulates Thymic Stromal Lymphopoietin Gene Expression via Protein Kinase Cdelta-p300-NF-kappaB Pathway in Keratinocytes under Inflammatory Conditions. *J Invest Dermatol*. 2019 May;139(5):1098-109.
98. Tamburini S, Shen N, Wu HC, Clemente JC. The microbiome in early life: implications for health outcomes. *Nat Med*. 2016 Jul 7;22(7):713-22.
99. Al Nabhani Z, Eberl G. Imprinting of the immune system by the microbiota early in life. *Mucosal Immunol*. 2020 Mar;13(2):183-9.
100. Constantinides MG, Belkaid Y. Early-life imprinting of unconventional T cells and tissue homeostasis. *Science*. 2021 Dec 10;374(6573):eabf0095.
101. Byrd AL, Deming C, Cassidy SKB, Harrison OJ, Ng WI, Conlan S, et al. *Staphylococcus aureus* and *Staphylococcus epidermidis* strain diversity underlying pediatric atopic dermatitis. *Sci Transl Med*. 2017 Jul 5;9(397).

ABSTRACT (IN KOREAN)

생후 초기단계의 특정 피부 공생 세균에 의해 유도되는 TSLP-제 2 형
선천 림프구의 활성화에 의한 알러지성 피부 염증 조절에 관한 연구

< 지도교수 유 지 환 >

연세대학교 대학원 의과학과

차 지 민

생후 초기 시기의 조직에 서식하게 되는 공생세균은 면역 체계를 조절하는 데 지속적으로 영향을 미치지만, 이 시기에 공생세균이 조절하는 피부의 면역 체계의 병리생리학적인 역할은 잘 알려져 있지 않다. 우리는 이와 관련해서 생후 초기 시기의 마우스 피부에 포도상구균인 스타필로코쿠스 렌투스¹가 서식하며 제2형 선천성 림프구 세포의 활성을 일으킴으로써 성인기에서 발생하는 아토피 피부염의 병증을 촉진한다는 것을 밝혔다. 생후 초기의 마우스 피부에서 공생 세균이 피부 각질세포에서 유도하는 TSLP가 생후 초기의 특정시기에 피부의 제2형 선천성 림프구 세포의 활성을 증가하게 한다. 구체적으로, 스타필로코쿠스에 속한 종들은 트립토판의 대사산물로 인돌-3-알데하이드를 생성하고 이 것으로 TSLP를 유도하여 제2형 선천성 림프구 세포의 활성을 일으킨다. 또한, 우리는 생후 초기 시기의 스타필로코쿠스 렌투스-TSLP-제2형 선천성 림프구 세포 활성화기전이 공생세균에 대한 노출 시기가 늦을 때는 일어나지 않는 것을 입증하였다. 이 연구를 통하여 우리는 생후 초기의 공생 세균과 피부의 상호작용이 성인기의 제2형 선천 면역 반응에 핵심적인 역할

을 수행한다는 것을 강조한다.

핵심 되는 말: 알레르기성 피부 질환, 아토피 피부염, 생후 초기 시기, 제2형 선천성 림프구 세포, 면역 각인, 피부 공생 세균, 스타필로코쿠스, 트립토판 대사산물